INTERNATIONAL JOURNAL FOR NUMERICAL METHODS IN FLUIDS, VOL. 1, 171–204 (1981)

THE CAUSE AND CURE (!) OF THE SPURIOUS PRESSURES GENERATED BY CERTAIN FEM SOLUTIONS OF THE INCOMPRESSIBLE NAVIER–STOKES EQUATIONS: PART 2

R. L. SANI

CIRES/NOAA, University of Colorado, Boulder, Colorado, U.S.A.

P. M. GRESHO AND R. L. LEE

Lawrence Livermore National Laboratory, Livermore, California, U.S.A.

D. F. GRIFFITHS

University of Dundee, Dundee, Scotland

M. ENGELMAN

CIRES/NOAA, University of Colorado, Boulder, Colorado, U.S.A.

SUMMARY

The spurious pressures and ostensibly acceptable velocities which sometimes result from certain FEM approximate solutions of the incompressible Navier–Stokes equations are explained in detail. The concept of pressure modes, physical and spurious, pure and impure, is introduced and their effects on discretized solutions is analysed, in the context of both mixed interpolation and penalty approaches. Pressure filtering schemes, which are capable of recovering useful pressures from otherwise polluted numerical results, are developed for two particular elements in two-dimensions and one element in three-dimensions. The automatic pressure filter associated with the penalty method is also explained. Implications regarding the effect of spurious pressure modes on accuracy and ultimate convergence with mesh refinement are discussed and a list of unanswered questions presented. Sufficient numerical examples are discussed to corroborate the theory presented herein.

KEY WORDS Finite Element Navier–Stokes Incompressible Flows Penalty Methods Pressure Filters

CONTENTS

IV. GENERALIZATION TO OTHER ELEMENTS 172
A. Theory 172
B. Applications 173
1. Bilinear velocity–piecewise constant pressure element 173
2. Equal-order interpolation elements 174
3. Higher-order mixed interpolation elements 175
C. Filtering the spurious pressure mode in a higher-order element 177
D. Further discussion of the biquadratic element 178
V. REMARKS ON EARLIER THEORY AND THE PENALTY APPROACH 179
A. Admonitions regarding theoretical results 179
B. Pressure modes a la penalty 180

0271–2091/81/020171–34$03.40

Received September 1980
Revised January 1981

VI. NUMERICAL EXAMPLES 184
VII. DISCUSSION 197
A. General comments 197
B. Outstanding questions 200
VIII. CONCLUSIONS 201
ACKNOWLEDGEMENTS 202
REFERENCES 202

IV. GENERALIZATION TO OTHER ELEMENTS

While theoretical results (see, for example, Crouzeix and Raviart[21] for the steady Stokes equations and Jamet and Raviart[22] for the steady Navier–Stokes equations) have established existence, uniqueness, and even error estimates of the approximate solution using certain elements, that from other elements can, as illustrated in the previous section, suffer from nonuniqueness and even nonexistence. The latter arises due to the occurrence of spurious pressure modes in the pressure approximation space. In order to gain additional insight into such problems it is necessary to extend the previous investigation of (pure) pressure modes to more complicated mixed *and* equal-order interpolation elements and this leads to an investigation of the uniqueness and existence of the GFEM approximation of the problem in its natural function space setting.

A. *Theory*

The formulation of the discretized Stokes problem can be cast in the following form: Find $\mathbf{u}^h \in W_h$ and $p^h \in Q_h$ such that

$$(p^h, \nabla \cdot \mathbf{w}^h) = A(\mathbf{u}^h, \mathbf{w}^h), \tag{36}$$

$$(\nabla \cdot \mathbf{u}^h, q^h) = 0 \tag{37}$$

for all $\mathbf{w}^h \in W_{h,0}$, $q^h \in Q_h$. Here

$$(a, b) = \int_\Omega ab \tag{38}$$

and

$$A(\mathbf{u}^h, \mathbf{w}^h) = \int_\Omega (\nabla \mathbf{w}^h)^T : \mathbf{S}(\mathbf{u}^h), \tag{39}$$

where S_{ij} is defined in (lc). W_h is a finite dimensional space of C^0 vector functions on Ω; $W_{h,0}$ is the subspace with vanishing components on those parts of the boundary on which the associated velocity components are specified. Finally, Q_h is a finite dimensional subspace of $L_2(\Omega)$ which itself is the space of all square integrable functions on Ω. The usual GFEM subspaces Q_h are either piecewise continuous (C^0) polynomials or piecewise discontinuous (C^{-1}) polynomials. The previous considerations on the linear velocity–constant pressure element can be recovered and generalized by investigating the uniqueness and existence of the GFEM solution.

First, the uniqueness question can be addressed by assuming that two solutions $(\mathbf{u}_1^h p_1^h)^T$ and $(\mathbf{u}_2^h p_2^h)^T$ exist. If

$$\mathbf{v}^h \equiv (\mathbf{u}_1^h - \mathbf{u}_2^h) \quad \text{and} \quad \hat{p}^h \equiv (p_1^h - p_2^h), \tag{40}$$

it follows from (36) and (37) that

$$A(\mathbf{v}^h, \mathbf{w}^h) = (\hat{p}^h, \nabla \cdot \mathbf{w}^h) \tag{41}$$

and

$$(\nabla \cdot \mathbf{v}^h, q^h) = 0 \tag{42}$$

for $\mathbf{v}^h \in W_{h,0}$, $\hat{p}^h \in Q_h$ and all $\mathbf{w}^h \in W_{h,0}$, $q^h \in Q_h$. A permissible specific choice is $(\mathbf{w}^h, q^h) = (\mathbf{v}^h, \hat{p}^h)$ and then (41) and (42), yield

$$A(\mathbf{v}^h, \mathbf{v}^h) = (\hat{p}^h, \nabla \cdot \mathbf{v}^h) \tag{43a}$$

and

$$(\nabla \cdot \mathbf{v}^h, \hat{p}^h) = 0. \tag{43b}$$

Since $A(\mathbf{v}^h, \mathbf{v}^h)$ is a positive definite quadratic form, it follows that $\mathbf{v}^h = \mathbf{0}$. (If the imposed boundary conditions are (f_t, f_n) specified *everywhere*, then $A(\mathbf{v}^h, \mathbf{v}^h)$ is only semi-definite and $\mathbf{v}^h$ equals a constant vector which implies that the velocity field is nonunique due to rigid body modes. This case is disallowed herein.) Therefore, the velocity field of the GFEM Stokes problem is *unique*. Then, setting $\mathbf{v}^h = \mathbf{0}$ in (41) and (42), uniqueness of the pressure field follows from

Condition A:

For all $\mathbf{w}^h \in W_{h,0}$,

$$(\nabla \cdot \mathbf{w}^h, p^h) = 0 \quad \textit{must} \text{ imply} \quad p^h = 0. \tag{44}$$

(The matrix analogue of (44) is $\mathbf{W}^T\mathbf{C}\mathbf{P} = 0$ for all vectors $\mathbf{W}$). If solutions to (44) exist with $p^h \neq 0$ (i.e. if Condition A is violated), the GFEM solution is nonunique; this nonuniqueness occurs as pressure modes—even though a *unique* velocity field is obtained.

It is noteworthy that the latter condition is also a restriction appropriate to the GFEM Navier–Stokes problem because it is generated by setting $\mathbf{v}^h = \mathbf{0}$ and the nonlinear terms vanish. The hydrostatic pressure mode obviously violates Condition A and, being acceptable physically, can be overlooked by recasting Condition A to read $p_h = \text{constant}$. Condition A is a special case (weaker version) of a result due to Brezzi[23] regarding existence and uniqueness for saddle point variational problems (see also Raviart[24]) and one of its consequences is that the computation of the eigenvalues of an element matrix as, for example, carried out by Olson and Tuann[3] is insufficient for the investigation of pressure modes.

When pressure modes exist, solvability conditions must also be satisfied by the GFEM system. These are generated by setting $(\mathbf{w}^h, q^h)^T = (\mathbf{0}, p^h_{mi})^T$, in (36)–(37), which leads to

Condition B:

$$(\nabla \cdot \mathbf{u}^h, p^h_{mi}) = 0; \qquad i = 1, 2, \ldots, n \tag{45}$$

where n is the total number of pressure modes p^h_{mi}. If this condition is violated, the associated GFEM system is inconsistent and has no solution. This is the generalization of (25), which was presented in association with the 4-node element.

B. *Applications*

1. *Bilinear velocity–constant pressure element.* The utilization of this alternative technique can be first illustrated by applying it to the previously considered case of the 4-node element,

the essential details of which have already been presented in Section III C. (see also Sani *et al.*[14]). The earlier description of situations in which hydrostatic and/or CB modes exist (the vanishing of the right-hand sides of (19) and/or (20), respectively) provides concrete examples of nontrivial pressure fields which violate Condition A. Finally, the solvability constraints previously generated for this element can be duplicated here by applying Condition B to these pressure modes (an exercise we leave to the reader).

2. *Equal-order interpolation elements.* In order to illustrate the application to equal-order interpolation elements, the C^0 bilinear velocity–bilinear pressure (C^0 or C^{-1}) interpolation will now be considered. For clarity and simplicity, we will consider meshes composed of straight parallel lines. In the discontinuous pressure case, the pressure representation employed here *and* hereafter utilizes Gauss point pressure nodes (located at the element centroid for the piecewise constant pressure element and at the 2×2 Gauss points for the bilinear pressure elements). In order to demonstrate the existence of pressure modes, it is only necessary to demonstrate a violation of Condition A. An isoparametric finite element is used and the quadrilateral elements in Figure 9 are mapped onto the reference square $[-1,-1]\leq(\xi,\eta)\leq[1,1]$. A violation of Condition A can be demonstrated by setting

$$p_i^h = D_i\xi\eta, \qquad \mathbf{w}^h = \begin{pmatrix} C_1 \\ C_2 \end{pmatrix}\phi(\xi,\eta),$$

where $p_i^h \in Q_h$ is the bilinear portion of the pressure in element i, D_i is an arbitrary constant in element i, and $\phi(\xi,\eta)$ is the appropriate velocity basis function.

For this case, application of (44) to the four-patch of Figure 9(a) leads to

$$\int_\Omega p^h \nabla\cdot\mathbf{w}^h = \sum_{i=1}^{4}\int_{\Omega_i} p_i^h \nabla\cdot\mathbf{w}^h$$
$$= \sum_{i=1}^{4} D_i\left[C_1\int_{-1}^{1}\int_{-1}^{1}\xi\eta(\alpha_i+\beta_i\eta)\,d\xi\,d\eta + C_2\int_{-1}^{1}\int_{-1}^{1}\xi\eta(\gamma_i+\delta_i\xi)\,d\xi\,d\eta\right]=0, \quad (46)$$

where α_i, β_i, γ_i and δ_i are constants associated with the mapping of element i into the reference square. Note that the integrals are identically zero for *arbitrary* constants (C_1, C_2, D_i) because all integrands are odd functions in either ξ or η. By restricting the index i in (46) to 2 or 1, one generates the form of the integral for a typical boundary two- or one-patch, respectively. Therefore, the same conclusion holds in these cases. Consequently, Condition A is violated not only in the C^0 bilinear pressure approximation case, but also in

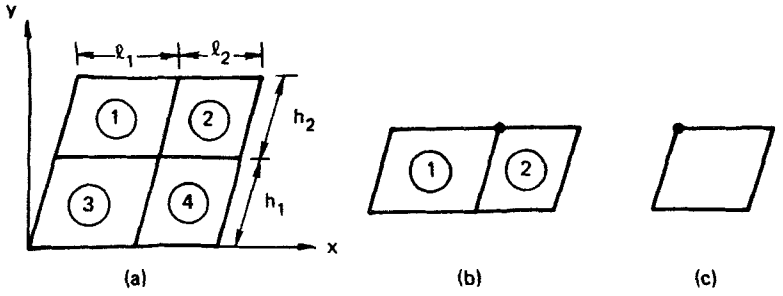

Figure 9. Sample patches of elements

the discontinuous (C^{-1}) bilinear approximation case. (The pressure mode $p_i^h = D_i\xi\eta$ corresponds to a C^0 approximation if the magnitude of D_i is the same for all elements but its sign is different for any two elements sharing a side; otherwise, p_i^h is a piecewise discontinuous (C^{-1}) approximation. Similar reasoning can be applied to the functions $p_i^h = D_i\xi$ or $p_i^h = D_i\eta$ which appear below.) Moreover, here the violation of Condition A and hence the occurrence of at least one spurious pressure mode is *independent* of the prescribed velocity boundary conditions because the boundary one-and two-patch results (velocity basis functions which would be associated with boundary nodes) are independent of C_1 and C_2.

Replacement of p^h appearing in the integral in (46) successively by $D_i = \text{const.}$, $D_i\xi$, and $D_i\eta$ can be used to further establish that at least the physical hydrostatic pressure mode, a spurious plane 'ξ-wave' pressure mode and a spurious plane 'η-wave' pressure mode, respectively, are also possible. In the latter two cases, Condition A is not violated automatically because of an odd integral as in the $\xi\eta$-mode case, but by satisfaction of certain constraints by these waves. In these cases, violation of Condition A on a 'four-patch' (Figure 9(a)) requires that

(1) for $p_i^h = D_i\xi$: $D_1 = D_4$, $D_3 = D_2$;

(2) for $p_i^h = D_i\eta$: $D_1 = D_2$, $D_3 = D_4$.

Condition (1) is satisfied by a ξ-wave on any four-patch in the grid and Condition (2) is similarly satisfied by the η-wave. The inclusion of a one-and two-patch test, which reflects the specification of normal or tangential forces on the boundary, establishes that the ξ-wave and η-wave pressure modes can be suppressed if the force normal to the wave form is specified on a portion of the boundary. Consequently, in general, multiple degeneracies must occur when using this element to simulate flows in which the velocity is specified everywhere on the boundary. In fact, on sufficiently large meshes, we have numerically encountered seven spurious pressure modes in one case and 80 in another. The C^{-1} bilinear pressure case is even more degenerate (and cannot even yield a velocity solution) because of an excess of continuity constraints compared to momentum equations; this is analogous to what happens if full quadrature is used on the equivalent of the '**B** matrix' in the penalty formulation.

Finally, the situation using equal interpolation with higher-order elements must be even more chaotic and we see no reason to pursue it.

3. *Higher-order mixed interpolation elements*

In the case of the higher-order C^0 biquadratic velocity and either C^0 or C^{-1} bilinear pressure interpolation, the additional types of basis functions with one-and two-patch support which must be added to those depicted in Figure 9 are displayed in Figure 10.

Construction of the integral in (44) with an appropriate velocity basis function ϕ leads to the following requirements for a violation of Condition A with $p_i^h = D_i\xi\eta$:

a. 4-*Patch* (*Figure* 9(*a*))

$$h_2(D_1 + D_2) - h_1(D_3 + D_4) = 0,$$
$$l_1(D_1 + D_3) - l_2(D_2 + D_4) = 0.$$

A translationally invariant solution requires that D_i depend only on geometrical characteristics of element i and hence the only such family of solutions appears to be $D_i = E/A_i$ where

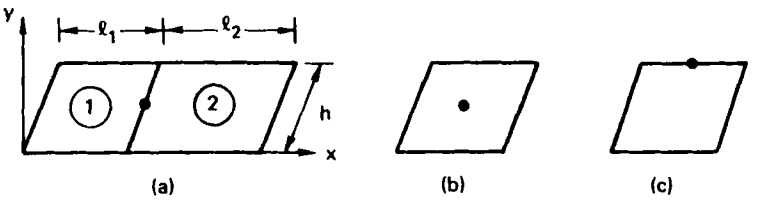

Figure 10. Sample patches of 9-node elements

E is an arbitrary constant and A_i is the area of element i. Note that the D_i's are all the *same* sign and hence a C^{-1} approximation space Q_h is required in order for a pressure mode to exist.

b. 2-*Patch* (*Figure* 10(*a*))

$$l_1 D_1 - l_2 D_2 = 0$$

A solution here is again of the form $D_i = E/A_i$ where E is an arbitrary constant.

c. 1-*Patch* (*Figure* 10(*b*))

The integral is identically zero and Condition A is violated independently of the value of D_i's.

d. 2-*Patch boundary elements* (*Figure* 9(*b*))

(i) No Specified Velocities

$$D_1 + D_2 = 0,$$

$$l_1 D_1 - l_2 D_2 = 0.$$

Here $D_1 = D_2 = 0$ and Condition A is always satisfied.

(ii) Normal Velocity Specified:

$$D_1 = -D_2$$

Here a C^0 pressure approximation space is required.

(iii) Tangential Velocity Specified

$$l_1 D_1 - l_2 D_2 = 0$$

Here $D_i = E/A_i$ and a C^{-1} pressure approximation space is required.

e. 1-*Patch boundary elements* (*Figures* 9(*c*) *and* 10(*c*))

Condition A is always satisfied.

A perusal of the foregoing results, with the requirement that all of the pertinent (as determined by boundary conditions) patch tests must be satisfied in order to demonstrate a violation of Condition A, allows one to conclude that in a domain of quadrilateral elements with the tangential component of velocity specified *everywhere* on the boundary, at least one spurious pressure mode will exist with a C^{-1} pressure approximation space.

A more complete analysis of the problem requires a straightforward extension of the foregoing analysis to the functions $p_i^h = \text{const.}$, $p_i^h = D_i\xi$ and $p_i^h = D_i\eta$. Since any bilinear

pressure on an element can be represented as a linear combination of these p-functions, one can then make additional statements about the number of spurious pressure modes. The result from this analysis which precludes any additional *spurious* modes is the constraint imposed by the 4-patch, e.g. for the ξ-mode,

$$h_2(D_1 + D_2) + h_1(D_3 + D_4) = 0,$$
$$l_1(D_3 - D_1) - l_2(D_2 - D_4) = 0,$$

which possesses *no* translationally invariant solution, i.e. D_i being only a function of the area of element i. Analysis of the η-mode leads to similar results. Thus, such mode forms *cannot* violate Condition A and lead to a spurious pressure mode; on the otherhand, $p_i^h = D_i =$ constant does violate Condition A if the normal velocity is specified everywhere on the domain and corresponds to the physical hydrostatic pressure mode.

Since the 'patch-tests' generate at most one spurious C^{-1} mode and no C^0 modes, it follows that mixed interpolation with a C^0 biquadratic velocity and C^0 bilinear pressure *cannot* exhibit spurious pressure modes while a C^{-1} bilinear pressure exhibits only the *one* spurious pressure mode previously described ($\xi\eta$), which can be suppressed by avoiding the specification of the tangential component of velocity *everywhere* on the boundary of the domain.

A similar analysis of the C^0 8-node serendipity velocity element leads to the following conclusions: (i) C^0 bilinear pressure cannot exhibit any spurious pressure modes, (ii) C^{-1} bilinear pressure can exhibit at least three spurious modes, the $\xi\eta$-mode, the ξ, mode and the η-mode.

C. *Filtering the spurious pressure mode in a higher-order element*

In Galerkin–finite element simulations of the incompressible Navier–Stokes equations using biquadratic approximation for velocity, there are two ways to proceed in order to finally obtain useful pressure fields. One can select an element which exhibits no spurious pressure modes or one can develop a filter to extract a useful approximation to the physical pressure field from the polluted numerical results of an element which exhibits a spurious CB pressure mode—pure and impure—in complete analogy with the 4-node element. While the former may appear more desirable from the point of view of pressure modes, there are also good reasons for choosing the latter (see Gresho *et al.*[25] for a critique of the C^0 pressure element). Equal-order interpolation, as in our second example, with its multiple degeneracies, probably does not even warrant consideration, but our third example of C^0 biquadratic velocity–discontinuous bilinear pressure with its single spurious mode, appears to be a viable (and generally very good) element and will be used here as a vehicle for describing another filtering scheme.

Once the form of the (single!) pressure mode is known, a filter can generally be devised by realizing that the numerical pressure field will contain a spurious component which is proportional to this pressure mode. A useful pressure field can sometimes be obtained by requiring that it have no component in the closed subset $Z_h \in Q_h$ spanned by the pressure modes. The method we developed for the 9-node element generates such a filtered pressure by annihilating the spurious CB mode *elementwise*, based on the knowledge that $\mathbf{P}_c^e = (1, -1, 1, -1)^T/A_e$ for a rectangular element of area A_e, where the four Gauss points are labelled sequentially in a clockwise (or counter clockwise) manner (note the resemblence to the CB mode on a 4-*patch* of 4-node elements). This is accomplished by requiring the four filtered Gauss point pressures on each (rectangular—the only type considered theoretically)

element to satisfy $P_1 - P_2 + P_3 - P_4 = 0$, which constrains the filtered pressure variation on an element to possess no component proportional to the elementwise variation of the $\xi\eta$-pressure mode (the filtered pressure is linear rather than bilinear). The resulting filtered pressures (P_i^f) are given by

$$P_i^f = \tfrac{1}{4}(3P_i + P_{[i+1]} - P_{[i+2]} + P_{[i+3]}), \qquad i = 1, 2, 3, 4, \tag{47}$$

where [ ] indicates an index modulo 4. These filtered pressures apply at the same four Gauss points as the original pressures and are still describable by the same C^{-1} basis functions (which of course now effectively degenerate to the form $\psi_i = a + b\xi + c\eta$); hence in this case the pressures are filtered but *not* smoothed. This filter provided useful pressure fields in all the numerical examples considered during our investigation (for both pure and impure modes). It is noteworthy (at least for pure CB grids) that these filtered pressures are 'physical' in the sense that they are the pressures 'seen' by the momentum equations (the $\xi\eta$-portion of the pressure is annihilated by the **C** matrix).

Similar ideas can presumably be useful in dealing with other elements generating spurious pressure (at least in those cases which exhibit a single, describable, spurious mode); however, it is noteworthy that the C^0 bilinear velocity–piecewise constant pressure element is a case in which an elementwise filtering procedure is apparently not appropriate (i.e. 'smoothing to the nodes' is also required).

D. *Further discussion of the biquadratic element*

To conclude this section, we point out some additional properties and consequences of the CB mode for the biquadratic, 2×2 Gauss point bilinear pressure element; as stated earlier, our analysis of this element has been limited to grids composed of rectangles (of arbitrary sizes). The global CB constraint equation is formed in the usual way ($\mathbf{P}_C^T\mathbf{C}^T\mathbf{U} = 0$), leading to (see equation (14))

$$\sum_{i=1}^{M}\left(\sum_{k=1}^{4}(-1)^{k+1}C_i^k\right)\Big/A_i = 0 \tag{48}$$

where C_i^k represents the kth continuity equation on the ith element (that obtained from the kth Gauss-point Galerkin equation, $C_i^k = 0$, $k = 1, \ldots, 4$), A_i is the area of that element, and there are M elements in the grid. As we observed from our analysis and discussion of the 4-node element, this spurious constraint equation contains several implications: (i) it is always satisfied by any (consistent) numerical solution; (ii) it leads to a CB mode when the imposed boundary conditions duplicate it (e.g. contained flows always exhibit a CB mode—either pure or impure); (iii) it imposes a constraint on the tangential velocities if any f_t boundary conditions are employed, and finally; (iv) it can lead to an ill-posed algebraic system if the applied boundary conditions violate it. An example of such violation can again best be demonstrated via the example of the lid-driven cavity with contained flow; if $u = u_0$ for nodes $3, \ldots, 2N-1$, where there are N elements across the lid (and $u_1 = u_{2N+1} = 0$ for contained flow), the constraint equation gives (for an odd *or* even grid)

$$(u_0 - 2u_2)/l_1 = (u_0 - 2u_{2N})l_N = 0,$$

where l_1, l_N are the lengths of the first and last elements, respectively. Hence, as with the bilinear element, the velocities to be imposed at nodes 2 and $2N$ must be selected carefully; e.g. if $l_1 = l_N$, $u_2 = u_{2N} = u_0/2$ will again suffice.

Also noteworthy is that $\sum_{k=1}^{4} C_i^k = 0$, $i = 1, \ldots, M$, which is implicit in the discretized system, generates element-level mass balances.

Ostensibly the 3-D version of this element (triquadratic velocity on a 27-node brick with trilinear pressure at the $2 \times 2 \times 2$ Gauss points) would, like its simpler counterpart (8-node brick), exhibit multiple (and perhaps unfilterable) CB modes.

Finally, we should point out that there are some *a priori* 'cures' for the CB problems with the 9-node element: (i) if the C^{-1} pressure is approximated linearly $(a + b\xi + c\eta)$ rather than bilinearly, there is no spurious pressure mode (results thus far from this element are encouraging;[19] however, the same linear pressure approximation in conjunction with the 8-node serendipity element can generate two spurious pressure modes); (ii) an equivalent, and more cost-effective procedure would employ the penalty method (again using the same, '3-node' linear pressure approximation) or the newly-developed 'approximately divergence-free element' by Griffiths.[26] In 3-D, we conjecture that again only a C^{-1} linear pressure approximation, $p^h = a + b\xi + c\eta + d\zeta$, would preclude CB modes; in this case, the price may be higher in that there are then relatively few continuity constraints[25] (by a factor of 2) compared with the trilinear (C^{-1}) pressure approximation, although results thus far are again encouraging.[19]

V. REMARKS ON EARLIER THEORY AND THE PENALTY APPROACH

A. *Admonitions regarding theoretical results*

Numerous theoretical investigations of the conventional Galerkin Finite Element Method (GFEM) as well as its penalty analogue (PGFEM) applied to the primitive variable form of the Navier–Stokes equations and their Stokes limit have appeared in the literature. For example, Crouzeix and Raviart[21] and Jamet and Raviart[22] considered the GFEM and Bercovier[16,27,28] considered additionally the PGFEM; a review of these topics is contained in Girault and Raviart.[29]

Focusing first on the GFEM formulation, these analyses provide hypotheses under which the scheme converges to a unique solution as well as error estimates. Crouzeix and Raviart[21] and Jamet and Raviart[22] consider a finite element mesh composed of nondegenerate triangles and provide both general results and results for specific elements; Bercovier[27] extended these results to the PGFEM (see also Reddy[30]). Most of these results, including existence and uniqueness, are ostensibly applicable to the Lagrange family of quadrilateral elements. However, our analyses indicate that the existence of pressure modes, i.e. nonuniqueness in the approximate pressure field on certain meshes, precludes a direct application of their results. Moreover, as demonstrated during the analysis of the 4-node element and the C^0 biquadratic velocity–C^{-1} bilinear pressure element, the solvability constraints imposed on the discrete problem by the spurious pressure modes can force the *allowable* boundary conditions to be mesh dependent. The latter raises fundamental questions relating to the convergence of these methods. The answer to these questions appears to lie in the basic hypothesis which is violated by the presence of spurious pressure modes in the pressure approximation space.

In all the analyses it appears that one of the basic hypotheses violated by the existence of pressure modes is either (a) for every $\psi^h \in Q_h$ whose integral over Ω is zero, there is a $\mathbf{v}^h \in W_{h,0}$ such that

$$\nabla_h \cdot \mathbf{v}^h = \psi^h \tag{49}$$

or alternatively (b) there exists a $k>0$ such that

$$\sup_{\mathbf{v}^h \in W_{h,0}} \frac{(\nabla_h \cdot \mathbf{v}^h, \psi^h)}{\|\mathbf{v}^h\|_{W_{h,0}}} \geq k \|\psi^h\|_{Q_h} \tag{50}$$

for all $\psi^h \in Q_h$. (The discretized operator ∇_h is defined as in Crouzeix and Raviart[21] by requiring $(\nabla_h \cdot \mathbf{v}^h, \psi^h) = (\nabla \cdot \mathbf{v}^h, \psi^h)$ for all $\psi^h \in Q_h$ (see also Appendix I). Thus, here it represents the Q_h projection of the operator $[\nabla \cdot]$ operating in $W_{h,0}$. Also, the norms $\| \|_{Q_h}$ and $\| \|_{W_{h,0}}$ are defined as in Bercovier.[27] If spurious pressure modes exist in the pressure approximation space Q_h (any physical hydrostatic mode can easily be suppressed by requiring the pressure to integrate to zero over Ω), then neither of the two hypotheses is satisfied since by definition of a pressure mode, p_c^h,

$$(\nabla_h \cdot \mathbf{v}^h, p_c^h) = 0 \tag{51}$$

for all $\mathbf{v}^h \in W_{h,0}$. (See also Carey[31].) But, using (49) for example, leads to $\int_\Omega (p_c^h)^2 = 0$, which would require $p_c^h = 0$. This dilemma can be resolved by realizing that the approximate pressure field generated by the GFEM in Q_h, while *not* unique, can still in some cases represent an approximation to the continuum pressure field if the approximate pressure field is constrained to possess zero component in Z_h, i.e. the null space of the discretized gradient operator, $\mathbf{C}$, which is spanned by the pressure modes. (See Fortin,[20] Brezzi[23] and Bercovier[27].) That is, the approximate pressure must be appropriately filtered as described, for example, in the preceding sections. In this case, one might expect the GFEM to converge to the unique (possibly up to an additive constant) continuum pressure field as the mesh is refined since this pressure can be shown to be in L_2, the space spanned by Q_h in the ultimate mesh refinement. Brezzi[23] presents necessary and sufficient conditions to ensure existence of an approximate solution; Fortin[20] gives some practical procedures to ensure satisfaction of (50). Song *et al.*[32] have additionally addressed the case in which the LBB constant (k, in (50)) is mesh-dependent.

In the presence of pressure modes one must proceed very carefully, both when interpreting the numerical results with their spurious pressures, and in presenting theoretical results. For example, Theorem 2 as presented in Bercovier and Engelman[16] appears to be invalid for the C^{-1} bilinear pressure element on a regular mesh because of the existence of a spurious pressure mode. Their numerical simulations do not clearly reflect the presence of this pressure mode, apparently because the penalty approach has a 'built-in' pressure mode filter which is discussed in the next section. A conventional GFEM solution employing the ostensibly identical pressure approximation space would lead to a very acceptable velocity field but (depending, as usual, on boundary conditions) a frequency completely spurious pressure field which, before filtering, would violate their comparison theorems.

The illustration of the inconsistent discretized system generated during the discussion of the 4-node element shows that additional complications can arise when pressure modes are present. As pointed out by Fortin,[20] one must question the very convergence of the GFEM (and also the PGFEM) in such cases.

B. *Pressure modes a la penalty*

In this section we attempt to correlate theory and experience when the penalty method is employed using the two elements previously considered via mixed interpolation (the 4-node element and the 9-node, C^{-1} bilinear pressure element). We will also elucidate the 'automatic built-in CB minimizer' associated with the penalty method. We first note that

there is no pure CB (formally) via the penalty approach (it is another impure mode); the penalty eigenvalue corresponding to what would be a pure CB is perturbed from zero like $O(1/\lambda)$.

1. *Analytical*

Beginning with the penalty 'equation of state,' $p^h = -\lambda \nabla \cdot \mathbf{u}^h$, we form

$$\int_\Omega p_m p^h = -\lambda \int_\Omega p_m \nabla \cdot \mathbf{u}^h, \tag{52}$$

where p_m is a pressure mode. If a (pure) pressure mode (or modes) would exist using mixed interpolation (MI), then the right-hand side of (52) must vanish by virtue of Condition B (45); hence

$$\int_\Omega p_m p^h = 0; \qquad m = 1, 2, \ldots, n, \tag{53}$$

is satisfied by the approximate pressure field from a penalty calculation for each pressure mode which would exist using MI (i.e. the penalty pressure has no projection onto the subspace spanned by pressure modes). For example, if a hydrostatic pressure mode would exist using MI, then the penalty method sets the 'arbitrary' constant via $\int_\Omega p^h = 0$ (this can also be derived via a global mass balance argument).

Penalty results are often somewhat polluted by oscillatory pressures which 'look like' CB's (while absent *globally*, via (53), a 'CB-like' mode is still present locally). Hence, assuming we can express the numerical result as the sum of a 'physical' pressure (p_p) and a CB pressure, p_c,

$$p^h = (p^h - a p_c) + a p_c \equiv p_p + a p_c \tag{54}$$

Equations (53) and (54) can be used (in principle) to obtain the pressure mode amplitude, a, in terms of the (unfortunately generally unknown) physical pressure, as

$$a = -\int_\Omega p_p p_c \Big/ \int_\Omega p_c^2 \tag{55}$$

Shortly we will use these results to explain the automatic CB minimizer associated with the penalty method, but first we digress slightly to suggest an alternative interpretation: If we require the penalty pressures to satisfy

$$\int_\Omega (p^h)^2 = \text{minimum}, \tag{56}$$

it is easy to show, via (54), and minimizing the integral with respect to the CB coefficient a (here $n = 1$ in (53)), that the result is again (53) and (55). This result appears to be related to the 'near minimization' of $\int_\Omega (\nabla \cdot \mathbf{u}^h)^2$ from the penalty version of the stokes functional,

$$F(\mathbf{u}^h) = \mu \int_\Omega (\nabla \mathbf{u}^h)^T : [\nabla \mathbf{u}^h + (\nabla \mathbf{u}^h)^T] + \lambda \int_\Omega (\nabla \cdot \mathbf{u}^h)^2; \tag{57}$$

the minimization of this functional gives the penalty velocity field and, for large λ, approximately minimizes $\int_\Omega (\nabla \cdot \mathbf{u}^h)^2$ or, equivalently, $\int_\Omega (p^h)^2$.

2. *Discretized*

The discretized version of $p^h = -\lambda \nabla \cdot \mathbf{u}^h$ is (4c) and the corresponding version of (52) is

$$\mathbf{P}_m^T \mathbf{M} \mathbf{P} = \lambda (\mathbf{U}^T \mathbf{C} \mathbf{P}_m \times \mathbf{P}_m^T \mathbf{g}), \tag{58}$$

where $\mathbf{P}$ is the vector of numerical pressures. The right-hand side of (58) vanishes if the pressure mode $\mathbf{P}_m$ would exist using MI; hence, under these conditions,

$$\mathbf{P}_m^T \mathbf{M} \mathbf{P} = 0, \qquad m = 1, 2, \ldots, n, \tag{59}$$

which is the discrete analogue of (53). In actual computations, however, round-off effects lead to $\mathbf{P}_m^T \mathbf{M} \mathbf{P} = O(\lambda e)$ where e is the unit round-off level (e.g. for $\lambda \cong 10^8$ and $e \cong 10^{-14}$, $\lambda e \approx 10^{-6}$). (If the boundary conditions preclude pressure modes using MI, then the penalty pressures agree with those from MI to $O(1/\lambda)$.)

Limiting (temporarily) subsequent discussion to the CB mode on rectangular elements for simplicity, we will show how (59), and the corresponding discretized form of (55) can be used to assess the built-in penalty treatment of this mode. Writing

$$\mathbf{P} = (\mathbf{P} - a\mathbf{P}_c) + a\mathbf{P}_c \equiv \mathbf{P}_p + a\mathbf{P}_c, \tag{60}$$

where $\mathbf{P}_p$ is the approximate (and unknown) vector of 'physical' pressures and $\mathbf{P}_c$ is the CB vector, we obtain, analogous to (55),

$$a = -\mathbf{P}_c^T \mathbf{M} \mathbf{P}_p / \mathbf{P}_c^T \mathbf{M} \mathbf{P}_c. \tag{61}$$

(a) *The 4-node element*

Using the fact that $M_{ij} = A_i \delta_{ij}$ and $P_{c_i} = \pm 1/A_i$ in (59) leads to

$$\sum_{\text{Red}} P_i = \sum_{\text{Black}} P_i; \tag{62a}$$

Equation (62a) is satisfied by the numerical penalty pressures and may be interpreted as the built-in CB filter a la penalty. Further clarification results from (61), which gives the amplitude of the CB pressure mode as

$$a = \pm \left(\sum_{\text{Red}} P_{p_i} - \sum_{\text{Black}} P_{p_i} \right) \Big/ \sum_{i=1}^{M} (1/A_i), \tag{63a}$$

where P_{p_i} is the (unknown) physical pressure on element i. We will return to this equation after discussing

(b) *The 9-node element*

For this element we have (for rectangles), $M_{ij} = A_i \delta_{ij}/4$ and $P_{c_i} = (1, -1, 1, -1)^T/A_i$, and (59) yields

$$\sum_{i=1}^{M} (P_1^i - P_2^i + P_3^i - P_4^i) = 0, \tag{62b}$$

where P_1^i is the penalty pressure at the first Gauss point on element i (etc.) and there are M elements. This is the automatic penalty CB 'filter' for the 9-node element and is always satisfied by the numerical results. Similarly, from (60) and (61),

$$a = \pm \tfrac{1}{4} \sum_{i=1}^{M} (P_{p_1}^i - P_{p_2}^i + P_{p_3}^i - P_{p_4}^i) \Big/ \sum_{i=1}^{M} (1/A_i), \tag{63b}$$

where $P^i_{p_k}$ is the (unknown) physical pressure at the kth Gauss point of element i. It is noteworthy that if (and only if) we apply the (elementwise) $\xi\eta$-filter to the pressures obtained from the penalty method, the results agree with those from MI (also after filtering of course) to $\sim O(1/\lambda)$; i.e. as mentioned previously, there is always some (small) local $\xi\eta$-component in the penalty pressures (which is *not* annihilated by the **C** matrix).

While it may not be obvious that the CB component is 'minimized' from (62) and (63), further insight may be gained from (63) if we restrict ourselves to a unit square domain of M equal-sized square elements of area $A = h^2$ (for which $M = 1/A$). For this case we obtain

$$a = A^2\left(\sum_{\text{Red}} P_{p_i} - \sum_{\text{Black}} P_{p_i}\right) \tag{64a}$$

for the 4-node element and

$$a = A^2 \sum_{i=1}^{M} (P^i_{p_1} - P^i_{p_2} + P^i_{p_3} - P^i_{p_4})/4 \tag{64b}$$

for the 9-node element. We now consider the effect of grid refinement; in particular, we wish to consider $h \to 0$. In this limit, the differences in *adjacent* 'physical' pressures in each of these equations can be shown (via Taylor series) to approach zero like $O(h^2)$, since, using (64b) for example,

$$\lim_{h\to 0} (P^i_{p_1} - P^i_{p_2} + P^i_{p_3} - P^i_{p_4})/4 = h^2 \frac{\partial^2 P^i_p}{\partial x\, \partial y}\bigg|_o + O(h^4), \tag{65}$$

where 'o' represents the point at the centre of the four nodes in question. Thus, inserting (65) into (64) gives, in general,

$$a = A^2h^2 \sum_{i=1}^{M} \left[\frac{\partial^2 P^i_p}{\partial x \partial y}\bigg|_o + O(h^2)\right] = O(A^2h^2M) = O(h^4). \tag{66}$$

Hence, since the CB amplitude goes like h^{-2}, the numerical penalty pressure, from (60), contains a CB component which decreases like $O(h^2)$ and it follows that each element (i.e. 4-node or 9-node) inherently provides a useful filter which suppresses the CB component as the mesh is refined.

For an impure CB mesh, this analysis may be combined with a perturbation analysis, as in Appendix II, to lead to the same overall result. Finally, it is noteworthy that the penalty method, in essence, automatically applies the filters which we (painfully) developed for mixed interpolation!

While not apparent from the above analysis, in practice it seems that the penalty filter is particularly effective for the 9-node element—so much so that some who have been using this penalty element (Heinrich,[33] Bercovier[34]) were not even aware of the existence of a CB mode. On the other hand, Hughes *et al.*,[9] who use the 4-node element in the penalty approximation, are well aware of pressure oscillations and have been using one of our early filters[10] to smooth the pressures (and here, as with the 9-node element, the filtered penalty pressures generally agree with the filtered MI pressures to $O(1/\lambda)$).

Finally, we point out that the penalty results are also susceptible to ill-posedness (in some sense) in that, if $(\mathbf{P}_c, \mathbf{g}) \neq 0$ for MI when a CB mode exists, the analogous penalty result will give useless velocities and pressures $O(\lambda)$; *cf.* (58).

VI. NUMERICAL EXAMPLES

In this section we present seven examples selected from the several hundred numerical experiments conducted during this study. These examples illustrate some of the items detailed in the previous sections.

Example 1. *Pure CB mode on a special mesh*

The mesh displayed in Figure 11 is an example of a special mesh configuration which can support a pure CB-mode when the 4-node element is employed. The mesh outlined entirely by solid lines displays a CB-mode when the problem is one in which normal and tangential velocities are specified at both inlet and outlet (with $u = v = 0$ on the top and bottom boundaries) while a specification of the tangential velocity, v, and normal traction, f_n, at the outlet requires that two of the elements at the outflow be modified as shown by the dashed lines. The construction of the mesh is a direct, but tedious, application of the ideas presented in Section III B and while such meshes appear to be very special, they significantly increase the probability of encountering slightly impure modes. In this example a small pivot of $O(10^{-15})$ was encountered during the course of the Gaussian elimination procedure which heralds the occurrence of the pure CB mode since the specification of f_n at the outflow precludes the physical hydrostatic mode. While the numerical results displayed acceptable velocities for such a coarse mesh, the pressures exhibited a definite CB-mode of magnitude $\sim \pm 6{\cdot}4$ superimposed on a physical pressure whose largest magnitude was ~ 6—a result which is unacceptable without filtering.

The results of filtering the numerical pressures by means of Schemes 1, 2 and 3 are displayed in Table I for $f_n = 0$ at the outlet. It is noteworthy that Schemes 1 and 2 yield similar results and exhibit the proper symmetry about the midplane while Scheme 3 is noticeably different and even unsymmetrical. The latter suggests that Scheme 3, the element area weighted scheme, is inferior and either Scheme 1 or 2 should be employed. However, we have found that Scheme 3 does yield acceptable results in most cases, especially when coupled with grid relaxation since it produces 'sufficiently good' pressures and is easy to implement (see Example 5).

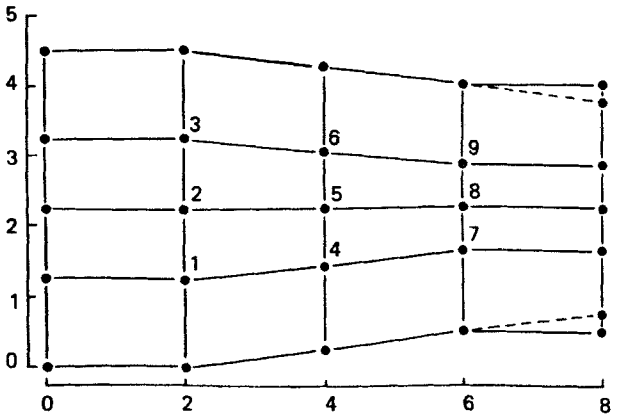

Figure 11. A special mesh which exhibits a pure CB mode

Table I. Filtered pressure from example 1

Node	Scheme 1	Scheme 2	Scheme 3	Bdy. pressure
1	5·3498393	5·3449216	5·2853930	6·27696
2	5·2834499	5·2834499	5·2834499	6·25065
3	5·3498393	5·3449216	5·4342014	6·33917
4	4·2187777	4·2187777	4·4181408	5·43836
5	4·1525227	4·1525227	4·1525227	5·29512
6	4·2187777	4·2187777	4·0926227	2·72315
7	2·5376785	2·5509268	2·5966438	0·73827
8	2·3985714	2·3985714	2·3985714	0·55279
9	2·5376785	2·5509268	2·5966438	0·15101

The filtered pressures at the nine nodes on the lower half of the boundary, numbered consecutively from the midnode of the left inlet, are also displayed in Table I. The linear extrapolation technique described in Section III F under Scheme 2 was combined with Scheme 2 to generate the filtered boundary pressures—which appear to be quite acceptable. It is also noteworthy, as previously mentioned, that this linear extrapolation technique can be used in conjunction with any of the filtering schemes.

Example 2. Consistent and inconsistent systems

This example illustrates consistent and inconsistent systems generated via the GFEM or PGFEM technique and some of their significant features. The results of the numerical experiments displayed in Table II are appropriate to the lid-driven cavity problem with the mesh of various sized rectangles illustrated below and in Figure 13 (the domain is square and 3 units long in each direction; it is discretized using 36 linear or 9 quadratic elements), a system which possesses a pure CB mode for the 4-node element and the 9-node element with C^{-1} bilinear pressure. As discussed earlier (Section III D, generalized to Condition B of Section IV and extended to the PGFEM in Section VB), the algebraic problem associated with the discretized system can be inconsistent if the CB constraint equation is violated. Under the 4-node element in Table II, Cases 1a,b and Cases 3a,b illustrate typical results obtained for consistent systems, and in particular, for systems similar to those detailed in Section III D. The velocity field in each case satisfies the discretized continuity equation, the GFEM and PGFEM solutions agree to $O(1/\lambda)$, and the pressure field, while exhibiting a pressure mode in the GFEM case, can be filtered to yield acceptable results. Also presented in Table II for Cases 1a,b is the pressure difference $(P_C - P_A)$ which is obtained by filtering the numerical pressures, illustrating reasonably close agreement between the GFEM and PGFEM results. In contrast, inconsistent systems (Cases 2a,b) display nonsatisfaction of the discretized continuity equation and concomitantly large pressures.

The same phenomena occur for the 9-node element with discontinuous bilinear pressure and are illustrated under '9-node element' in the table.

Example 3. Impure pressure mode

Portions of this example were summarized during our theoretical discussion of impure CB modes, but more details are worthwhile since those results, taken alone, appear to be rather

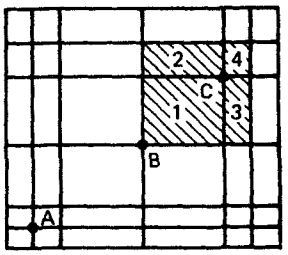

Table II. Selected results from the lid-driven cavity problem

	Velocity $(u, v)^T$			Pressures	
	A	B	C	2 1	4 3
1. Top B.C. $(u = 1, 1, 1, \ldots, 1, 1, 1)$					
a. GFEM	$-2{\cdot}727\times10^{-3}$ $2{\cdot}727\times10^{-3}$	$-1{\cdot}391\times10^{-1}$ $2{\cdot}720\times10^{-13}$	$-4{\cdot}838\times10^{-2}$ $-1{\cdot}848\times10^{-1}$	6·341 3·458 $(P_c-P_A)=0{\cdot}606$	−0·349 8·804
b. PGFEM ($\lambda = 10^8$)	$-2{\cdot}727\times10^{-3}$ $2{\cdot}727\times10^{-3}$	$-1{\cdot}391\times10^{-1}$ $8{\cdot}929\times10^{-9}$	$-4{\cdot}838\times10^{-2}$ $-1{\cdot}848\times10^{-1}$	0·6606 0·3265 $(P_c-P_A)=0{\cdot}615$	1·617 0·574
2. Top B.C. $(u = 0, 1, 1, \ldots, 1, 1, 0)$					
a. GFEM	−4·500 −7·000	−1·967 −0·495	1·140 −0·454	$O(10^{15})$	
b. PGFEM ($\lambda = 10^8$)	$-1{\cdot}063\times10^{-1}$ $-1{\cdot}496\times10^{-2}$	$-2{\cdot}791\times10^{-1}$ $1{\cdot}154\times10^{-8}$	$-1{\cdot}744\times10^{-1}$ $-4{\cdot}173\times10^{-1}$	$O(10^7)$	
3. Top B.C. $(u = 0, 0{\cdot}5, 1, \ldots, 1, 0{\cdot}5, 0)$					
a. GFEM	$-1{\cdot}474\times10^{-3}$ $1{\cdot}474\times10^{-3}$	$-1{\cdot}882\times10^{-1}$ $3{\cdot}331\times10^{-16}$	$-7{\cdot}486\times10^{-2}$ $-3{\cdot}974\times10^{-1}$	−2·092 −0·781	5·636 −5·682
b. PGFEM ($\lambda = 10^8$)	$-1{\cdot}474\times10^{-3}$ $1{\cdot}474\times10^{-3}$	$-1{\cdot}882\times10^{-1}$ $7{\cdot}999\times10^{-9}$	$-7{\cdot}486\times10^{-2}$ $-3{\cdot}974\times10^{-1}$	1·564 0·238	1·381 0·611

II. 9-Node element	Velocity $(u, v)^T$			Pressures
	A	B	C	
1. Top B.C. $(u = 1, 1, 1, \ldots, 1)$				
a. GFEM	$3{\cdot}865\times10^{-3}$ $3{\cdot}463\times10^{-3}$	$-1{\cdot}384\times10^{-1}$ $-1{\cdot}4\times10^{-13}$	$-5{\cdot}962\times10^{-2}$ $-2{\cdot}122\times10^{-1}$	$O(1)$
b. PGFEM ($\lambda = 10^8$)	$-3{\cdot}865\times10^{-3}$ $3{\cdot}463\times10^{-3}$	$-1{\cdot}384\times10^{-1}$ $1{\cdot}568\times10^{-8}$	$-5{\cdot}962\times10^{-2}$ $-2{\cdot}122\times10^{-1}$	$O(1)$
2. Top B.C. $(u = 0, 1, 1, \ldots, 1, 1, 0)$				
a. GFEM	$-9{\cdot}180\times10^{-2}$ $-1{\cdot}138\times10^{-1}$	$-1{\cdot}658\times10^{-1}$ $-8{\cdot}034\times10^{-3}$	$-7{\cdot}025\times10^{-2}$ $1{\cdot}587\times10^{-1}$	$O(10^{14})$
b. PGFEM ($\lambda = 10^8$)	$-4{\cdot}641\times10^{-2}$ $-3{\cdot}348\times10^{-2}$	$-1{\cdot}911\times10^{-1}$ $-4{\cdot}734\times10^{-2}$	$-1{\cdot}767\times10^{-1}$ $-4{\cdot}589\times10^{-1}$	$O(10^7)$

Table III. Summary of numerical results for an impure CB mode

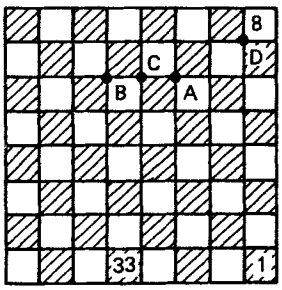

ε	X_A	Y_A
0	0·625	0·750
10^{-9}	0·625000001	0·750000002
10^{-6}	0·625001	0·750002
10^{-3}	0·625	0·752

I. (Top B.C.: $u = 0$ everywhere: no flow case)

ε	P_{Red}	P_{Black}	u's and v's	Smallest pivot
0	1·0(13*)	0·1449(13*)	$O(10^{-15})$	3×10^{-16}
10^{-9}	1·0(9)	0·6765(9)	$O(10^{-12})$	1×10^{-16}
10^{-6}	1·0(9)	0·9998(9)	$O(10^{-12})$	7×10^{-13}
10^{-3}	1·0(13)	0·9999(12)	$O(10^{-15})$	7×10^{-7}

II. (Top B.C.: $u = 1$ everywhere)

	ε	P_8	P_{33}	U_c	V's at centreline
	0	−21·035	0·5380	0·08046	$O(10^{-14})$
	10^{-9}	$1{\cdot}921\times10^{6}$(6*)	0·5385	0·08078	$O(10^{-4}$–$10^{-6})$
	10^{-6}	$3{\cdot}216\times10^{5}$(4)	0·6293	0·13427	$O(10^{-2}$–$10^{-3})$
	10^{-3}	$3{\cdot}356\times10^{2}$(1)	0·6290	0·13425	$O(10^{-2}$–$10^{-3})$
$P_1 = P_2 = 0$:	10^{-3}	13·536	0·3603	0·08033	$O(10^{-5}$–$10^{-4})$

	ε	U_A	U_B	U_D	V_D
	0	0·06157	0·06157	0·13448	−0·13448
	10^{-9}	0·06201	0·06167	0·13442	−0·13442
	10^{-6}	0·13542	0·07782	0·12503	−0·12503
	10^{-3}	0·13939	0·07779	0·12496	−0·12496
$P_1 = P_2 = 0$:	10^{-3}	0·06586	0·06187	0·13432	−0·13432

* Number of figures of agreement in pressure on red (or black) elements.

pessimistic with regard to the thus far elusive convergence proofs for the 4-node element. The experiments were performed on a unit square grid composed of 64 equal-sized (before the perturbation) 4-node elements, as depicted in the sketch associated with Table III. For both 'undriven' and 'driven' (Stokes flow, $u = 1$) cavities, we perturbed the mesh by moving node A (which defines ε) as shown in the table. The pressure on element 1 was fixed at 1·0 in all runs except that labelled $P_1 = P_2 = 0$. A perusal of Table III, which summarizes the

salient results, reveals the following:

Undriven cavity

(1) For the pure CB ($\varepsilon = 0$), the pressures are 1·0 on all red elements (element 1 is red) and ~0·145 on all black elements (the ratio of two unit round-off numbers from Gaussian elimination). The velocities are zero to machine accuracy.
(2) For $\varepsilon > \sim 10^{-6}$, the CB mode is absent and all pressures are essentially unity (velocities are still ≈ 0).
(3) As ε goes from 10^{-6} to 10^{-3}, the smallest pivot increases by six orders of magnitude (it, like the perturbed eigenvalue, varies like ε^2 in this range).
(4) $\varepsilon = 10^{-9}$ is in the 'transition' range (it is barely noticeable).

Driven cavity (same pivot behaviour of course).

(1) The pure CB case displays oscillatory pressures and the velocities display the appropriate symmetry (e.g. v is zero along the vertical centerline, $u_B = u_A$, etc.).
(2) For 'recognizable' perturbations ($\varepsilon > \sim 10^{-9} - 10^{-6}$), the pressure on the (unpegged) black elements varies like ε^{-1} and the velocities at and near the perturbed node are perturbed to $O(1)$ independent of ε, which also causes a disproportionate loss of symmetry.

A direct application of the internal constraint equation, (27), to this grid yields (using compass point notation with node A located (before the 'tweak') at the center of a 4-patch):

$$(u_E + u_W - u_N - u_S)\sin\theta - (v_E + v_W - v_N - v_S)\cos\theta = 0, \tag{67}$$

where $\theta = \tan^{-1}\Delta y_A/\Delta x_A$ is the angle associated with the perturbation of node A. This equation, which is indeed satisfied by our numerical results (at least for $\varepsilon = 10^{-6}$ and $\varepsilon = 10^{-3}$), and while derived from element mass balances, is quite extraneous and spurious (and is, appropriately, not satisfied by the $\varepsilon = 0$ solution). What was a redundant continuity equation for the pure CB mesh has become an extraneous internal constraint equation in the perturbed mesh.

Hence, all of the dire predictions of the impure CB theory are verified by these experimental results. More optimistic results, however, will be presented in Example 7.

The results shown in the last entry in Table III correspond to the idea discussed in Section III E wherein we peg two pressures, which sacrifices exact continuity on the two corresponding elements in favour of a regularization of the matrix. As shown in the table, the velocities are now indeed perturbed only to $O(\varepsilon)$; in addition, the impure CB is very small (we set $P_1 = P_2 = 0$ which is in a region of small ∇P, and thus even the raw element pressures look good; this will be further clarified in the next section) and the smoothed pressures display good, symmetric contours (see Figure 12(a)) which are indistinguishable from those obtained from the pure ($\varepsilon = 0$) CB run (in contrast to the somewhat distorted, unsymmetric isobars obtained from any of the three schemes when exact mass balances are enforced—see Figure 12(b)).

When we repeated the $\varepsilon = 10^{-3}$ experiment using the 'node-freeing' idea (which we introduce and discuss in the next section), we again observed a regular perturbation from the $\varepsilon = 0$ results (we freed a tangential node on the bottom of the cavity and set $f_t = 0$ there; the resulting CB-oscillation was quite small and the tangential velocity at the freed node was $O(\varepsilon)$).

Finally, we repeated these runs using the penalty method ($\lambda = 10^8$) for $\varepsilon = 0$ and $\varepsilon = 10^{-3}$ and obtained the following results: (i) the velocities agreed with those using mixed interpola-

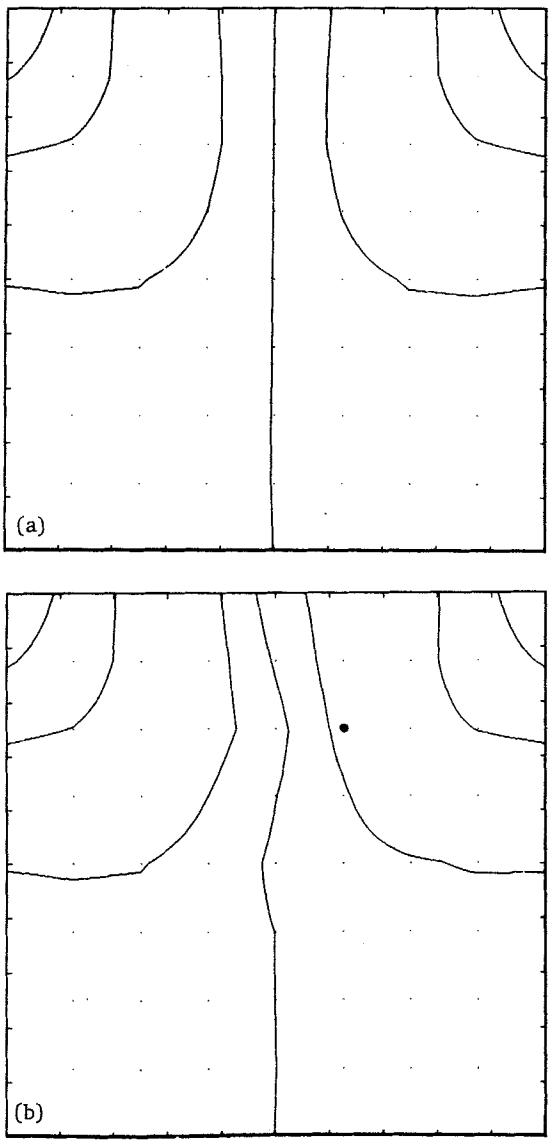

Figure 12. Isobars for the driven cavity, Example 3: (a) $\varepsilon = 0$, (b) $\varepsilon = 10^{-6}$ or 10^{-3}. Contour levels are 0, ±1, ±5, ±10

tion in the usual way (to $O(1/\lambda)$) which implies that impure modes are also harmful to penalty results; (ii) for $\varepsilon = 10^{-3}$ the raw pressures contained an impure CB pressure oscillation of $O(\pm 160)$, showing that the built-in penalty filter is more effective on meshes which would exhibit a pure CB using mixed interpolation (the $\varepsilon = 0$ penalty pressures looked very good).

These same 'tweaked node' experiments were also repeated with the 9-node element (C^{-1} bilinear pressure) on the same mesh (here, however, tweaking one corner node also required appropriate 'tweaks' to the nearest 8 affected neighbouring nodes) with somewhat similar results: (i) the impure mode ($\varepsilon = 10^{-3}$) caused fairly large (but not as large as with the 4-node element) velocity perturbations for both mixed interpolation and penalty; (ii) the CB pressure oscillations were large, $O(\pm 100)$ for $\varepsilon = 10^{-3}$, again for mixed and penalty (the $\varepsilon = 0$ penalty pressures again were unpolluted and looked quite good).

Example 4. *Comparison of filtered pressures*

In this example we compare the filtered pressures from the 9-node element (2×2 Gauss point pressures) with those from the built-in penalty method filter for the same element and for the (penalty) 4-node element. The test problem is (again) the 'leaky'-lid-driven cavity (Stokes flow; $u = 1$ across the top) on a 3×3 square grid (as in Example 2) of 9 biquadratic elements which are various-sized rectangles as shown in Figure 13; each 9-node element was

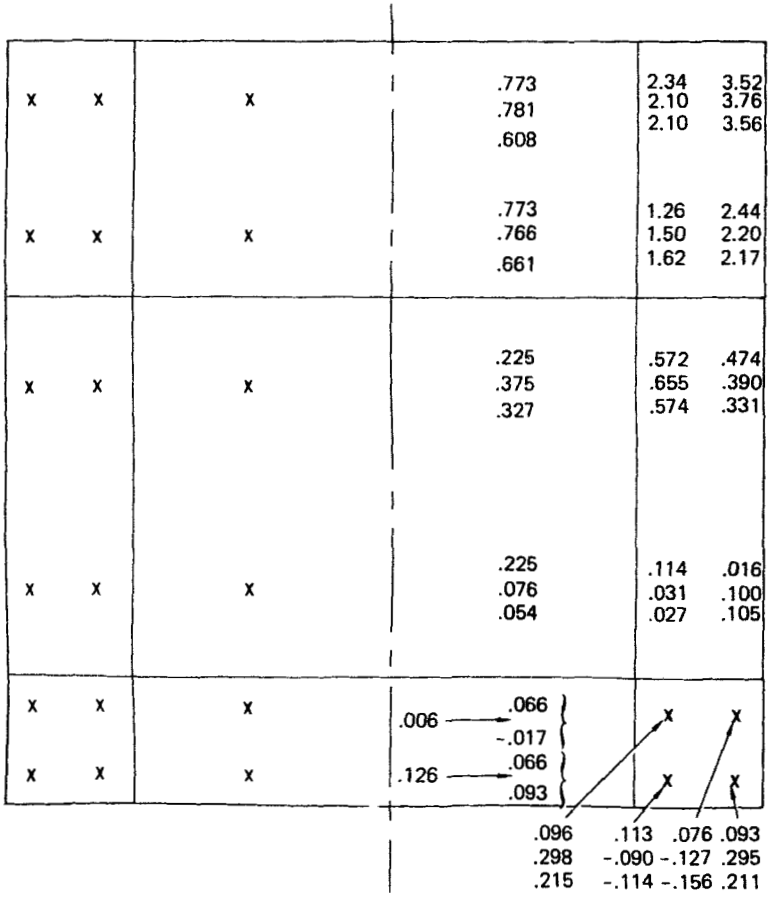

Figure 13. Pressures from a driven-cavity experiment

divided into four equal rectangles to generate the corresponding 36-element mesh of 4-node elements (the centroids of the 4-node elements are close to, but slightly displaced from, the Gauss points of the 9-node element). Since the mesh is symmetric, and the pressures satisfy $\int_\Omega p^h = 0$, only one-half of the pressures are displayed in Figure 13; the pressures at the Gauss points shown on the left-hand are the negative of those printed on the right-hand side. For the mixed interpolation case, the (pure) CB mode was first filtered, then the hydrostatic level was set to agree with that from the penalty case. The first entry at each 'node' is that from mixed interpolation with the xy-portion of the pressure field removed element-wise (the 9-node filter); the second entry is the 9-node penalty pressure, and the bottom entry is the 4-node penalty pressure.

It is seen that all pressures look fairly reasonable in the high pressure region and, considering the coarseness of the mesh, are quite agreeable with each other. The differences show up in the low pressure region wherein a 'lingering local impure CB' is present in both penalty results. Finally, as mentioned earlier, if the 9-node penalty pressures are processed with the xy-filter, the resulting pressures agree with the filtered mixed interpolation pressures to $\sim O(1/\lambda)$ and are the physical pressures in the sense that they are the only ones 'seen' in the momentum equations. Also, as the mesh is refined, we would expect the filtered pressures from MI to agree more and more closely with the penalty pressures for the 9-node element.

Example 5. *Performance of the CB filters on a highly distorted mesh*

Here we present more Stokes-driven cavity results, this time for a nonleaky cavity ($u_i = 0$, 0·5, 1·0, 1·0, . . . , 0·5, 0 across the top) and on a highly distorted unit square grid comprising

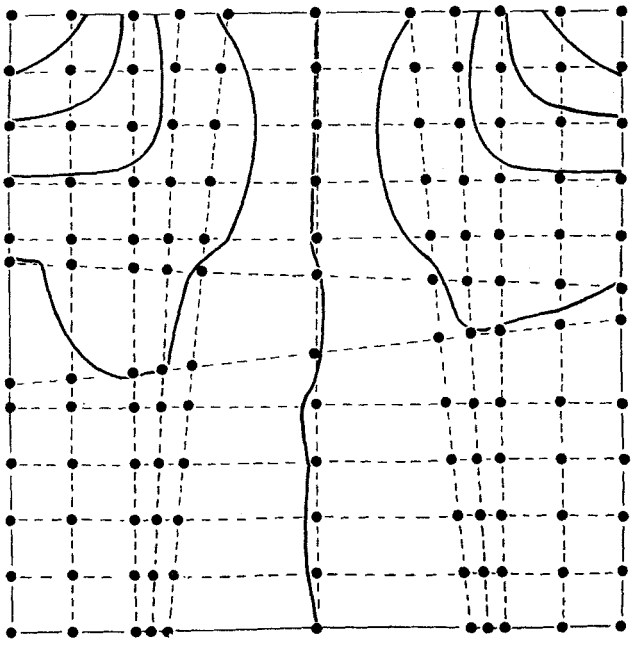

Figure 14. A mesh of distorted elements and isobars from Scheme 3

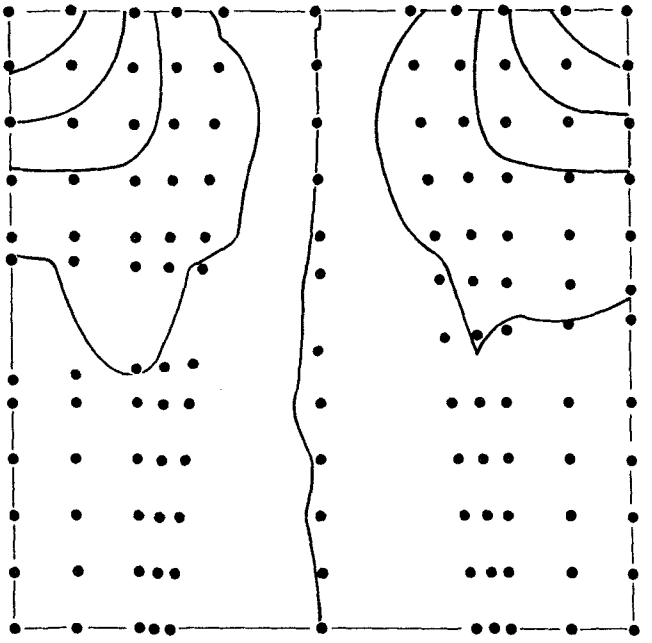

Figure 15. Isobars from Scheme 2

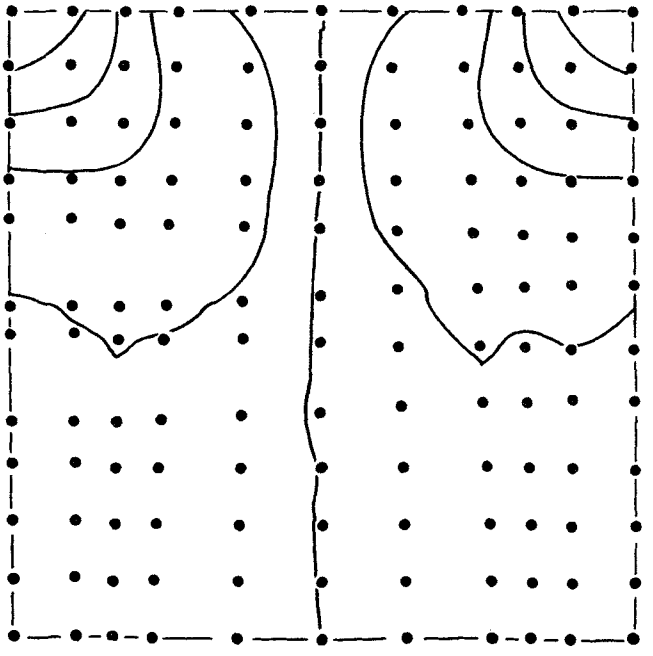

Figure 16. Isobars on a smoothed grid (Scheme 2)

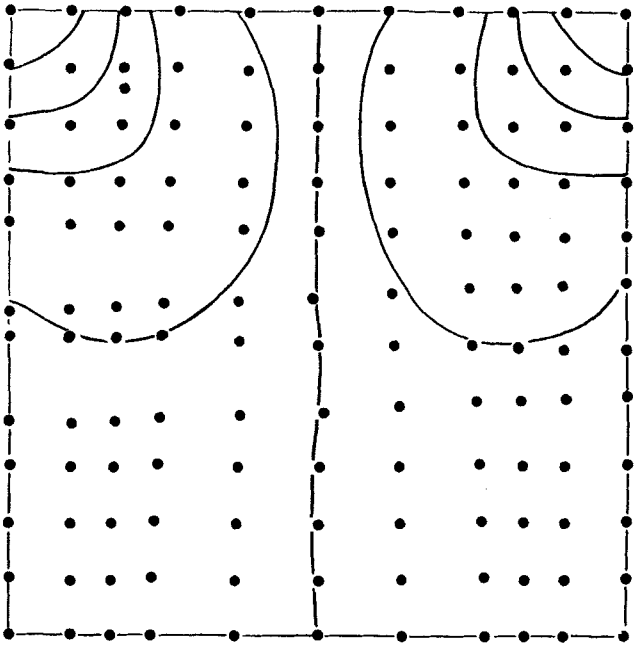

Figure 17. Isobars on a smoothed grid (Scheme 3)

110 4-node elements (Figure 14). This grid is probably quite far removed from a pure CB grid, although we can never really be sure (there were, however, no exceptionally small pivots). The raw pressures were noticeably oscillatory (one pressure was pegged at 1·0) and the velocity vectors looked reasonable. Figure 14 shows the original grid and the pressure contours obtained from Scheme 3 (the contour levels in all figures are 0, ±1, ±5, ±10, ±20). These contours, and those from Scheme 1 or Scheme 2 (the two are virtually indistinguishable—Figure 15), are rather jagged and unsymmetrical, although we should probably not expect much better from such a poor mesh and the more difficult boundary conditions. In Figures 16 (Scheme 2) and 17 (Scheme 3) we display the much improved results obtained by combining grid smoothing with pressure filtering and smoothing; the contours in Figure 17 are especially good. It appears that the simplest scheme (element area smoothing) applied to both the pressures and the nodes may be quite effective in the general case.

Finally, when we repeated this calculation with two pressures pegged, the results were generally little different, especially in the regions of significant velocities. The smoothed pressure contours were virtually indistinguishable from those when exact mass balances were enforced, thus suggesting that the 'trick' of pegging two pressures (or one, depending on boundary conditions) is really only useful when the impure mode is very close to a pure mode (*cf.* Example 3); it may, however, never be too harmful and sometimes quite beneficial.

Example 6. Simple analytic test case

An exact solution to the Stokes equations is $u = x$, $v = -y$, $p =$ constant, and represents colliding (or turning) flow, since the stream function is $\psi = xy$. We tested the 4-node element on this problem (on several grids) by applying the exact solution as a Dirichlet boundary condition. The results were encouraging in that the exact solution was obtained at the nodes for both pure and impure CB grids (equation (27) is identically satisfied by the exact solution). The 4-node element, on pure or impure grids, can converge—at least for some problems.

Example 7. Experiments with mesh refinement

In order to generate some experimental evidence relating to the potential convergence of the 4-node and 9-node (2×2 Gauss point pressures) elements, we performed several sets of experiments on a sequence of four meshes on the unit square. For the 4-node element, these were: 4×4, 8×8, 16×16 and 32×32. The 9-node element mesh used the same node locations (1/4 as many elements for each grid). In addition to these uniform girds, we also generated impure grids by perturbing either one or all of the internal nodes (the latter via a random number generator) for the 16×16 grid. These grids were employed on two problems, one rather easy (but with an analytic solution available) and the other more difficult (the driven cavity(!)).

(a) *A body force problem.* This problem has been previously studied by Song *et al.*[32] and is useful in that the analytic solution is available which, while not an exceptionally difficult solution (it is very smooth), does permit some quantitative error analysis. If the appropriate 'body force' terms are added to the right-hand sides of (1a), then an exact solution to (1a), (1b) which vanishes on the boundary of the unit square is

$$u = 2x^2(1-x)^2y)(1-y)(1-2y)$$
$$v = -2x(1-x)(1-2x)y^2(1-y)^2$$
$$p = x^2 - y^2$$

The (polynomial) body force term can be computed via $f = \nabla^2\mathbf{u} - \nabla p$.

Using the penalty formulation with $\lambda = 10^6$ and Dirichlet boundary conditions ($\mathbf{u} = \mathbf{0}$ on $\partial\Omega$), we present the results of these experiments in Figure 18 in the form of L_2 error norms, e.g.,

$$\|v\|_0^2 = \int_\Omega v^2$$

for both velocity and pressure. The curves in Figure 18(a) are those for a uniform mesh, but the results for a mesh with one tweaked node ($\varepsilon \cong 10^{-3}\, h$) are basically indistinguishable (this also applies to the 9-node results in Figure 18(b)). Hence, for this problem, the velocities appear to be converging at the appropriate rates. Similarly, the pressure for the 4-node element is converging at the ostensibly appropriate rate ($O(h)$). The only explanation we have (at this time) for the apparent superconvergence of the pressure for the 9-node element (where one might expect $O(h^2)$ in general), is that the problem is too 'easy' owing to smoothness and symmetry.

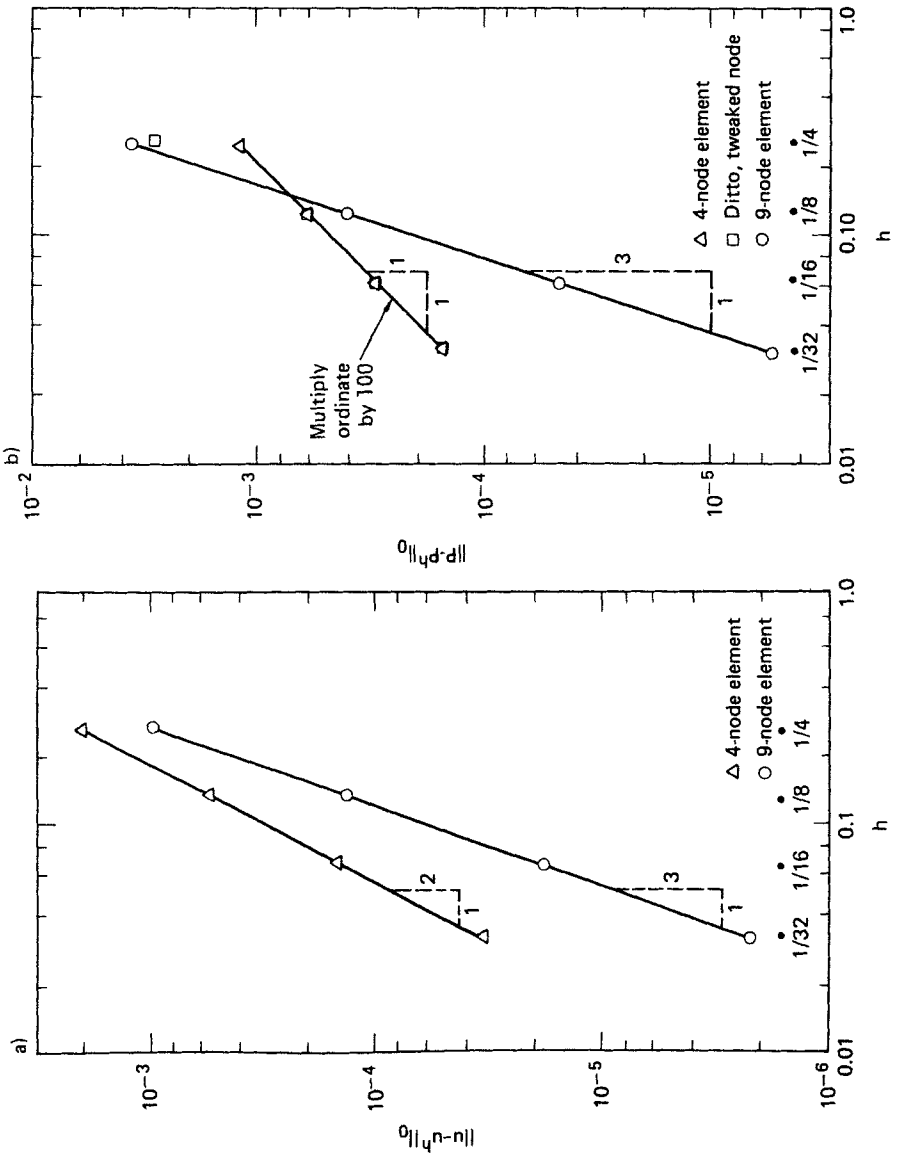

Figure 18. Convergence test results for the body force problem

There are several additional noteworthy points regarding these results (which have been independently verified by Malkus[35] for the 4-node element):

(i) Both elements appear to be converging with increasing mesh refinement, for pure and impure meshes, in both velocity and pressure, at least in the penalty version. For mixed interpolation, the pressure will of course diverge in L_2 (at least for pure CB meshes) if it is not filtered; the filtered pressures will presumably converge, although we have not done the calculations.

(ii) The CB component of the pressure is effectively suppressed via the penalty method, for both pure and impure CB meshes. (See also Figure 19, in which the CB amplitude—estimated via the Augen method[36] and labelled 'analytic problem'—goes to zero like $O(h^4)$ for the 4-node element, in apparent agreement with the theory (appropriately modified for the tweaked node) since $\partial^2 P/\partial x\,\partial y = 0$; for the 9-node element, the CB amplitude was too small to even detect. All results in Figure 19 are from tweaked node (impure CB mesh) runs; for $\varepsilon = 0$, the CB amplitude was too difficult to detect, even for the 4-node element—it is probably absent.)

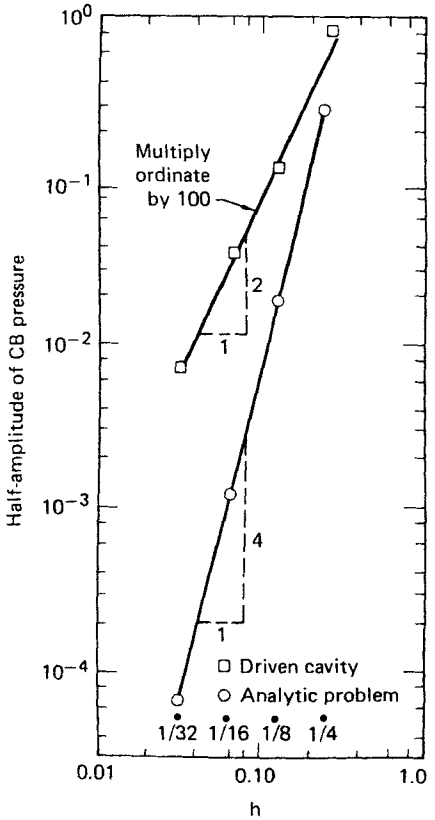

Figure 19. CB amplitude on slightly impure grid *vs* mesh refinement for two problems, both using the 4-node element

(iii) These results are at variance with those of Oden *et al.*, who computed[32] (*and* apparently predicted[37]) divergence in the pressure as the mesh is refined.

(b) *The driven cavity.* The same sequence of meshes was used for the leaky lid-driven cavity problem (penalty formulation; 4-node element) with the following results:

(i) The CB amplitude on the uniform mesh was almost too small to measure (at least for 16×16 and 32×32). For the impure mesh with one tweaked node ($\varepsilon\cong10^{-3}\,h$), the CB pressures, while large for coarse meshes, see Figure 19, were suppressed like $O(h^2)$ as the mesh was refined; again, substantiating the theory put forth in Section V B. Even when all internal nodes were randomly tweaked with the same (average) ε, the CB amplitude was similar to that with one tweaked node.

(ii) For one tweaked node, the velocity perturbations were $O(1)$ at essentially all nodes on the 4×4 mesh, and at only a few nodes in the neighbourhood of the tweak for the 8×8 mesh. For the 16×16 and 32×32 meshes, the velocity perturbations were very small ($\ll O(1)$) even near the tweaked node. When all nodes were perturbed on the 16×16 mesh, the velocity perturbations were still quite small—$O(10^{-3})$.

We also ran the 16×16 mesh using mixed interpolation and observed the following:

(i) With one node tweaked (two values of ε), the CB amplitude again varied like $1/\varepsilon$, but the velocities were only slightly perturbed—$O(10^{-3})$.

(ii) With all nodes tweaked, the velocity perturbations were again very small and the CB amplitude ($\sim\pm14$) agreed with that from the corresponding penalty result.

The net result from this series of experiments is that the deleterious effects of the spurious CB pressure mode and associated constraint equation appear to decrease nicely with mesh refinement.

VII. DISCUSSION

In this section we will elucidate several more of the points learned during this study and close by listing a number of things we did *not* learn.

A. *General comments*

1. The first (albeit not profound) item we address is the behaviour of the algebraic system when the consistency requirements (e.g. Condition B) imposed by pressure modes are not quite satisfied; a practical physical case occurs wherein the problem is described by specified inflow and outflow velocities in the presence of a hydrostatic mode (no f_n boundary conditions). If (25) is slightly violated, say via $(\mathbf{g}, \mathbf{P}_m)=\varepsilon\ll1$ where $\mathbf{P}_m$ is a pressure mode vector, then it can be shown that the solution to (4a), (4b) via Gaussian elimination will behave like

$$\begin{aligned}\mathbf{P}&=\mathbf{P}_0+\beta(\varepsilon/e)\mathbf{P}_m+O(\varepsilon),\\ \mathbf{U}&=\mathbf{U}_0+O(\varepsilon),\end{aligned}\tag{68}$$

where $(\mathbf{U}_0, \mathbf{P}_0)$ is the solution for $\varepsilon=0$, e is the unit round-off level, and β is a scalar of $O(1)$. Hence, as ε increases from zero, the pressure field rapidly becomes dominated by the null space eigenvector whose consistency condition is violated. If $\varepsilon\ll1$, the solution (68) may be 'acceptable,' but a 'large ε' violation ($\varepsilon\approx1$) would give useless results.

2. We have experimented with the idea of *a priori* CB minimization, the goal of which is to obtain useful pressures without filtering. The two schemes we shall describe are sometimes useful in situations wherein something is known about the solution to the physical problem.

To explain the first scheme, 'selective pressure specification,' we first suppose that both pressure modes are present, in which case the numerically computed pressure $\mathbf{P}_N$, can be represented as

$$\mathbf{P}_N = \mathbf{P}_P + \gamma_H \mathbf{P}_H + \gamma_c \mathbf{P}_c, \tag{69}$$

where $\mathbf{P}_p$ is the desired (physical) pressure, $\mathbf{P}_H$ is the hydrostatic mode, $\mathbf{P}_c$ is the CB mode, and γ_H, γ_c are generally arbitrary. Since it is permissible to specify two pressures, consider the effect of specifying $[\mathbf{P}_N]_R = P_{NR}$ on the Rth red element and $[\mathbf{P}_N]_B = P_{NB}$ on the Bth black element (or the corresponding two nodes for the 9-node element). This procedure in effect specifies γ_H and γ_c since (69) generates a 2×2 system whose solution is

$$\gamma_c = \frac{(P_{NB} - P_{NR}) - (P_{PB} - P_{PR})}{P_H(P_{CB} - P_{CR})}, \tag{70a}$$

where $P_H = 1$, $P_{CB} = 1/A_B$, $P_{CR} = -1/A_R$, and the value of γ_H is immaterial. Of course the physical pressures on the two selected elements, P_{PR} and P_{PB} are unknown; if they were known, however, it is clear that we could eliminate the CB mode ($\gamma_c = 0$) by setting $P_{NB} = P_{PB}$ and $P_{NR} = P_{PR}$. In the actual case, γ_c can be made 'small' as follows:

(i) Select adjacent elements for pressure specification (on two adjacent nodes in the same element if the 9-node element is considered).

(ii) Set $P_{NB} = P_{NR}$ (value immaterial; use 0); this makes $\gamma_c \sim (P_{PB} - P_{PR}) \sim \nabla P$, the 'actual' pressure gradient at the 'point' in question.

(iii) Select a region of the grid (for adjacent red/black pegging) where the pressure gradient is smallest (this is where qualitative knowledge of the solution would be useful).

If there is no hydrostatic mode, $\gamma_H = 0$ in (69) and the analogous procedure is to peg $[\mathbf{P}_N]_R = P_{NR}$ on the Rth red element (say) which leads to

$$\gamma_c = A_R(P_{NR} - P_{PR}). \tag{70b}$$

In this case γ_c can be minimized by picking R to be an element on that part of $\partial\Omega$ where f_n is specified; then, since $P_P \approx f_n$ in many cases,[17] P_{NR} is specified to be the value of the normal traction force specified for the Rth element (e.g. a common outflow boundary condition is $f_n \approx 0$; in this case one simply sets $P_N = 0$ on one of the elements along this boundary).

If the CB mode is slightly impure (such as might be obtained from an ostensibly rectangular mesh generated by a mesh generator code), then the same procedure may still be useful, but this time for an additional reason: it will regularize the matrix and lead to better velocity and pressure solutions, as discussed earlier.

The second scheme is called 'node-freeing' and differs in that, rather than reducing the number of continuity equations, we increase (by 1) the number of momentum equations. In particular, the 'trick' is to release the tangential velocity at one node on the boundary; i.e. change the imposed boundary condition at one node from 'U_t (tangential velocity) specified' to 'f_t (tangential shear) specified.' This serves the purpose of precluding the pure CB mode (matrix no longer singular) while still maintaining the desired value of U_t at the given node (it is automatically enforced by the CB boundary constraint equation—e.g. (14)). Whether or not this trick suppresses pressure oscillations again depends on some knowledge about the solution; in particular, the value of f_t at the node in question. In practice, the freed node should probably be selected in a region of minimum wall shear, and $f_t = 0$ employed (a large discrepancy between the imposed value of f_t and the 'desired' value will excite a CB pressure oscillation to the extent of the difference). This scheme too can be quite effective on a 'nearly pure' mode, again owing to matrix regularization. Donea *et al.*[38] have used a related trick

(freeing all tangential velocities during part of a time step) for solving the time-dependent Navier–Stokes equations, using the 'explicit' method outlined by Gresho *et al.*[17] (In our current 'explicit' 2-D and 3-D codes, we (PMG and RLL) do not resort to this trick, which must introduce some error; rather, we allow the CB to exist and filter it when pressures are desired.)

Both of these schemes, which were demonstrated to be effective in Example 3, are also applicable to the penalty method of solution and may be especially useful on the troublesome 'nearly pure' CB grids (the latter scheme is obviously easier to implement).

3. A potentially effective practical procedure for 'automatically' dealing with pure and impure CB modes is outlined below.

The situations encountered in practice may be classified as being of one of three types. These are (i) pure CB grids, (ii) small perturbations of CB grids and (iii) large perturbations of CB grids. Of the three, it is the second which creates the greatest practical difficulties. This is a consequence of the fact (discussed earlier) that an arbitrarily small perturbation of a pure CB grid can lead to $O(1)$ perturbations in the velocity field. An *a priori* classification of a given grid is *not possible* in general and thus an acceptable implementation of the two CB elements' must deal equally with all three cases. With this in mind, we tentatively propose the following strategy, which may well not be foolproof (nor always easy to implement). The element level matrices are loaded and the elimination (or factorization) method of solution applied in the usual manner except that we take advantage of the fact that the presence of pressure modes, whether physical or spurious, can usually be deduced from the behaviour of the pivots. A drop in pivot size to round-off level reveals the presence of a pure mode whereas a drop in pivot size by 'several' orders of magnitude is a strong indication of an impure pressure mode. (If either situation is encountered, the consistency or otherwise of the system can be checked by comparing the pivot size with the corresponding component of the source vector.) In both cases the pivotal value is reset to a suitably large value (10^{10} say) and the elimination process continued. Resetting the pivot in this way is tantamount to pegging the pressure to some arbitrarily small value on the appropriate element (or node). Finally, the computed pressure is smoothed in accordance with one of the procedures detailed earlier. The main advantage of this strategy is that the spurious grid-dependent internal constraint (usually present in small perturbations of CB grids) need not be satisfied. That is to say the problem has been regularized in these cases.

4. We believe that many discussions (and implementations) of the penalty method would be improved, and much of the aura of mystique and even suspicion which we still see exemplified by many onlookers eliminated, if notions of reduced quadrature 'tricks' were replaced by the more straightforward 'mixed interpolation via penalty' approach, beginning with the discretized version of the continuum equation, $p = -\lambda \nabla \cdot \mathbf{u}$. While it is true that this approach does necessitate (in general) the explicit introduction of the (clearly defined) basis functions for pressure, it is at once more appealing and, we believe, more general[19] Reduced quadrature, when equivalent (e.g. 4-node element or 9-node element with straight sides) could *then* be advocated as a slightly more cost-effective procedure.

5. The 'tweaked node' experiments presented in Examples 3 and 7 indicate the desirability of examining the spurious internal CB constraint, (27), more closely. We first return to (67) and consider its behaviour with mesh refinement. To this end we express the velocities at nodes N, S, E and W in terms of the central node (at its untweaked location) via Taylor series to obtain, as $h \to 0$, from (67),

$$h^2\left(\frac{\partial^2}{\partial x^2}-\frac{\partial^2}{\partial y^2}\right)(u \sin\theta - v\cos\theta) + O(h^4) = 0. \tag{71}$$

While the factor multiplied by h^2 is indeed spurious, it is the h^2 factor itself which is most important; viz. (71) implies that the spurious constraint equation actually *vanishes* like $O(h^2)$ with mesh refinement. This indicates that the constraint equation, while perhaps deleterious on a coarse mesh, becomes more and more innocuous as the mesh is refined and, in the limit, vanishes identically for any velocity field; i.e. even the exact solution satisfies (71) for $h \to 0$, which suggests that the potential barrier to convergence is automatically removed (the spurious constraint equation does not preclude convergence in velocity). A similar analysis is applicable to the spurious CB boundary constraint equation (13 or 14) and the results are also similar (the equation 'vanishes' as $h \to 0$).

This encouraging result can be generalized to an arbitrary mesh, and leads to a linear combination of the same types of expressions shown in (67), one for each node, with coefficients proportional to the departure of the given grid from the nearest (generally unknown) CB grid. The net effect, with grid refinement, is a linear combination of terms as in (71), each of which vanishes identically as $h \to 0$.

With this result, and our supporting numerical evidence, we offer the following hypotheses for both of the 'CB-prone' elements under consideration:

(i) The velocities will converge as $h \to 0$ for *any* mesh, for both mixed interpolation and penalty methods;

(ii) On a pure CB grid, the pressures from mixed interpolation will always retain an arbitrary amount of CB, even for $h \to 0$; hence the pressure can (and will) only converge after it is filtered (and smoothed if appropriate);

(iii) On an impure CB mesh, the pressures from mixed interpolation will converge as $h \to 0$ (and ε independent of h) with or *without* filtering;

(iv) The pressures from the penalty method will also converge, for pure or impure CB meshes, with or without filtering.

6. Returning to the boundary condition constraint equations for either the hydrostatic or the CB pressure modes (equation (25)), or both simultaneously, we make the following additional claims, which also re-emphasize the importance of (25): If an exact solution to the Navier–Stokes equations is used to specify Dirichlet boundary data via specified (exact) nodal values of $\mathbf{u}$ on $\partial\Omega$, the FEM approximation is ill-posed if these boundary conditions violate either of the pressure mode constraint equations and when the associated pressure mode exists for the given grid. Well-posedness (and convergence as $h \to 0$) may be recovered in (at least) two ways: (i) employ the natural boundary condition appropriate to the pressure mode in question over at least a portion of $\partial\Omega$ (even at just *one* node!); (ii) modify the Dirichlet boundary data in such a way (e.g. via a least squares adjustment) that the appropriate constraint equation(s) is satisfied. Of course, if the pressure mode is the CB mode and mixed interpolation is used, pressure convergence can only occur after the appropriate filter is employed.

7. More recent arguments based on the order of the velocity derivatives vis-a-vis the order of the pressure derivatives (Segal[39]) or on the number of discretized momentum equations vis-a-vis the number of continuity equations (Schneider *et al.*[40]) are still inadequate to explain the need for mixed-interpolation. Even inviscid flows (Euler equations) will display pressure modes if equal-order interpolation is employed, and the constraint (equation) ratio is in fact nearly optimum[25] using equal interpolation.

B. *Outstanding questions*

As is typical of research, this investigation has perhaps raised more questions than it has answered. Hence, in spite of the conjectures presented above, we conclude by posing some of our salient questions.

1. Convergence of the 4-node (and 9-node, C^{-1} bilinear pressure) elements, both before and after CB mode filtering:
   (a) For the general mesh of distorted, isoparametric elements?
   (b) In the presence of a pure CB pressure mode?
   (c) On a mesh which is a *small* perturbation from a pure CB mesh?
   (d) Effects of mesh 'regularization' (is it necessary?) such as red/black pressure pegging or node freeing (or the penalty approach, which is a regular perturbation of mixed interpolation)?
   (e) Effect of grid-smoothing (4-node element) on the pressure convergence?
2. For the 9-node element (C^{-1} bilinear pressure), of 'what use' is the 'xy'-portion of the pressure approximation, both in p^h and as a 'test function' for the momentum equations:
   (a) In the presence of a pure CB mode on a rectangular mesh (in which case the **C** matrix annihilates the effects of the xy-pressure variation elementwise)?
   (b) In the absence of a pure CB mode (e.g. when f_t boundary conditions are used on a rectangular mesh)?
   (c) On a general mesh, with curved isoparametric elements?
3. What is the relative 'accuracy' of the 9-node element using 3-node (C^{-1}) linear pressure, 4-node (C^{-1}) bilinear pressure and 4-node (C^0) bilinear pressure, only the second of which can display a CB mode? (Bercovier and Pironneau[41] have analysed the C^0 element on rectangular grids.)
4. Which of the two filters for the 9-node, C^{-1} bilinear pressure element (the element-wise xy-filter a la mixed interpolation or the automatic global filter a la penalty) is 'better' on a 'coarse' mesh?
5. What is the true nature and consequences of the impure CB mode associated with an f_t boundary condition?
6. Finally, what is the 'situation' for three-dimensional flow simulation?

VIII. CONCLUSIONS

1. There is only one nonspurious pressure mode—the hydrostatic mode—and it will occur using any element, any mesh, and boundary conditions which specify the normal velocity on all of $\partial\Omega$. Violation of the consistency condition associated with this null space eigenvector will occur if erroneous (or inconsistent) boundary data are specified.
2. The 4-node element and the 9-node element with C^{-1} bilinear pressure can each exhibit one spurious (pure) CB mode and an associated nonphysical constraint equation among the boundary velocities, violation of which will cause an ill-posed algebraic system. These CB modes can be successfully filtered by the procedures described herein.
3. These elements can also exhibit impure CB modes which are more difficult to deal with. The potential danger of these impure modes is very high (especially when they are 'nearly' pure and the mesh is 'coarse'), both numerically and theoretically. It is not generally possible, *a priori*, to determine the proximity of an impure mode to a pure mode, nor even whether a pure mode will exist.
4. The penalty analogue of these elements can also exhibit a related (impure) CB mode which is (partially) filtered automatically on coarse meshes; as the mesh is refined, the penalty filter becomes more effective and, in the limit, suppresses the CB mode altogether and in a manner which is analogous to the filters we developed for mixed interpolation (see also Malkus[42]).
5. The penalty method is equivalent to (in the sense of a regular perturbation) the

appropriate mixed interpolation analogue when implemented in the consistent manner described herein (and, more specifically, in Engelman *et al.*[19]).

6. The 9-node velocity element with C^0 bilinear pressure exhibits no spurious pressure modes. This is also true for the 9-node element using C^{-1} *linear* pressure approximation; this element is deserving of more attention, since it is also quite accurate.[19]
7. The 8-node (serendipity) velocity element with C^0 bilinear pressure exhibits no spurious pressure modes. The same element with C^{-1} bilinear pressure can exhibit three spurious pressure modes; if C^{-1} linear pressure is employed, this element can exhibit two spurious pressure modes.
8. Equal-order interpolation elements (C^0 pressure) exhibit many spurious pressure modes which do not appear to be filterable. (Equal-order interpolation with C^0 velocity and C^{-1} pressure is not even possible owing to an excess of continuity equations.)
9. Grid smoothing appears to be an effective procedure for improving the pressure accuracy for the 4-node element (and the corresponding 8-node trilinear element in 3-D).
10. The simplest 3-D element (8-node trilinear velocity, piecewise constant pressure) exhibits many spurious CB modes, all of which are filterable (at least when pure) by the same filter.
11. Many of these results apply to certain finite difference approximations, which are thus necessarily encumbered with spurious pressure modes.
12. Theoretical analyses of accuracy and convergence must consider the effects of the spurious boundary constraint equation and the spurious pressure modes (both pure *and* impure) when present.

ACKNOWLEDGEMENTS

We would first like to thank Dr. A. C. Hindmarsh (LLNL) for many useful and enlightening discussions as well as several supporting independent analyses during the entire course of this investigation. Dr. S. T. Chan (LLNL) deserves much of the credit for discovering, analysing, and filtering the CB modes in our 3-D code as well as providing general assistance. Finally, we are grateful to Dr. M. Bercovier (Hebrew University) for his helpful and constructive review of the manuscript.

Nancy Badal's patience with us as we struggled through many changes and several drafts of a long and difficult-to-type manuscript is also appreciated.

RLS would like to acknowledge support from both Lawrence Livermore National Laboratory and the U.S. Army Research Office (Grant DAAG29-79-6-0045).

This work was performed under the auspices of the U.S. Department of Energy by the Lawerence Livermore National Laboratory under contract No. W-7405-Eng-48.

REFERENCES

1. C. Taylor and P. Hood, 'A numerical solution of the Navier–Stokes equations using FEM technique, *Computers and Fluids*, **1**, 73–100 (1973).
2. P. Hood and C. Taylor, 'Navier-Stokes equations using mixed interpolation', in *Int. Symp. on Finite Element Method in Flow Problems*, Proceedings, Swansea, Wales (1974).
3. M. Olson and S. Tuann, 'Primitive variables versus stream function finite element solutions of the Navier–Stokes equations', in *Finite Elements in Fluids*, Volume 3, Wiley, Chichester, 1978, pp. 73–89.
4. G. D. Richards, 'Finite elements for incompressible flow', *M.Sc. Dissertation*, Dept. Math., University of Reading, UK (1978).
5. J. H. Argyris, P. C. Dunne, T. Angelopoulos and B. Bichat, 'Large natural strains and some special difficulties

due to non-linearity and incompressibility in finite elements', *Comp. Methods Appl. Mech. and Eng.*, **4**, 219–278 (1974).
6. J. C. Nagtegaal, D. M. Parks and J. R. Rice, 'On numerically accurate finite element solutions in the fully plastic range,' *Comp. Methods Appl. Mech. and Eng.*, **4**, 153–177 (1974).
7. O. R. Fabayo, 'Bilinear finite elements for incompressible flow', *M.Sc. Dissertation*, Dept. Math., University of Dundee, Scotland (1977).
8. P. A. Huyakorn, C. Taylor, R. L. Lee and P. M. Gresho, 'A comparison of various mixed interpolation finite elements in the velocity-pressure formulation of the Navier–Stokes equations', *Computers and Fluids*, **6**, 25–35 (1978).
9. T. J. R. Hughes, W. K. Liu and A. Brooks, 'Finite elements analysis of incompressible viscous flows by the penalty formulation', *J. Comp. Phys.*, **30**, 1–15 (1979).
10. R. L. Lee, P. M. Gresho and R. L. Sani, 'Smoothing techniques for certain primitive variable solutions of the Navier–Stokes equations', *Int. J. num. Meth. Engng.* **14**, 1785–1804 (1979).
11. M. Fortin, 'Numerical solution of steady state Navier–Stokes equations', in *Numerical Methods in Fluid Dynamics* (Ed. J. J. Smolderen), Agard Lecture Series No. 48, AGARD–LS–48 (1972).
12. W. E. Pracht and J. V. Brackbill, 'BAAL: A code for calculating three-dimensional fluid flows at all speeds with an Eulerian–Lagrangian computing mesh', *Los Alamos Scientific Laboratory Report LA–6342* (1976).
13. A. Chorin, personal communication and, 'On the convergence of discrete approximations to the Navier–Stokes equations', *Math. of Comp*, **23**, 341–353 (1969).
14. R. Sani, P. Gresho and R. Lee, 'On the spurious pressures generated by certain GFEM solutions of the incompressible Navier–Stokes equations', *Third Int. Conf. on Finite Elements in Flow Problems*, Proceedings, Banff, Alberta, Canada (1980).
15. C. Caldwell, Westinghouse Electric Corporation, Pittsburgh, PA, private communication (1979).
16. M. Bercovier and M. Engelman, 'A finite element for the numerical solution of viscous incompressible flows', *J. Comp. Phys.*, **30**, 181–201 (1979).
17. P. M. Gresho, R. L. Lee and R. L. Sani, 'On the time-dependent solution of the incompressible Navier–Stokes equations in two and three dimensions', in *Recent Advances in Numerical Methods in Fluids*, Pineridge Press, Swansea, U.K., 1980.
18. D. S. Malkus and T. J. R. Hughes, 'Mixed finite element methods—reduced and selective integration techniques: A unification of concepts', *Comp. Methods Appl. Mech. and Eng.*, **15**, 63–81 (1978).
19. M. Engelman, M. Bercovier, R. Sani and P. Gresho, 'Consistent vs. reduced integration formulations for penalty FEM solutions using several "old" elements and one new element', in preparation.
20. M. Fortin, 'An analysis of the convergence of mixed finite element methods', *RAIRO*, **11**, R–3, 341–354 (1977).
21. M. Crouzeix and P. A. Raviart, 'Conforming and nonconforming finite element methods for solving the stationary Stokes equations I', *RAIRO Serie Mathematiques*, R–3, 33–76 (1973).
22. Jamet, P. and P. A. Raviart, 'Numerical solition of the stationary Navier–Stokes equations by finite element methods', *Lecture Notes in Computing Sci. Part* 1, 193–223, (Ed. G. Goos and J. Herimanis), Springer-Verlag, 1974.
23. Brezzi, F., 'On the existence, uniqueness and approximation of saddle point problems arising from Lagrangian multipliers', *RAIRO*, **8**, R–2, 129–151 (1974).
24. Raviart, P. A., 'Finite element methods and Navier–Stokes equations', in *Computing Methods in Applied Sciences and Engineering, Part 2*, (Ed. Glowinski and Lions), Lecture Notes **91**, Springer-Verlag, New York (1979).
25. Gresho, P., R. Lee, S. Chan and J. Leone, 'A new finite element for Boussinesq fluids', *Third Int. Conf. Finite Elements in Flow Problems*, Proceedings, Banff, Alberta, Canada (1980).
26. Griffiths, D. F., 'An approximately divergence-free 9-node velocity element for incompressible flow', in preparation.
27. Bercovier, M., 'Perturbation of mixed variational problems. Application to mixed finite element methods', *RAIRO Analyse numerique*, **12**, 211–236 (1978).
28. Bercovier, M., 'A family of finite elements with penalisation for the numerical solution of Stokes and Navier–Stokes equations', *Information Processing 77*, (Ed. B. Gilchrist), 97–101, North-Holland (1977).
29. Girault, V. and P. A. Raviart, 'Finite element approximations of the Navier–Stokes equations', *Lecture Notes in Math.*, No. 749, Springer-Verlag (1979).
30. Reddy, J. N., 'On the accuracy and existence of solutions to primitive variable models of viscous incompressible fluids', *Int. J. Engng Sci.*, **16**, 921–929 (1978).
31. Carey, G., 'Some remarks on finite element analysis of viscous flow problems', *Third Int. Conf. on Finite Elements in Water Resources*, Proceedings, Univ. of Mississippi, Oxford, Miss. (1980).
32. Song, Y., J. T. Oden, and N. Kikuchi, 'Discrete LBB-conditions for RIP-finite element methods', *TICOM Report 80–7*, Texas Institute for Computational Mechanics, University of Texas at Austin (1980).
33. Heinrich, J., personal communication.
34. Bercovier, M., personal communication. (We have since learned, however, that he and Engelman actually achieved filtered pressures, since only centroid values were reported.)
35. Malkus, D., 'Convergence of Penalty/FEM solutions for the Stokes problem', Ill. Inst. of Tech. *Research Report No. 81–1*, for NSF Grant No. CME 80–17549 (1981).

36. Eyeball method.
37. Oden, J. T., 'RIP-methods for Stokesian flows', TICOM *Report 80-11*, Texas Institute for Computational Mechanics, University of Texas at Austin (1980).
38. Donea, J., S. Giulani and A. Laval, 'Accurate explicit finite element schemes for conductive–Convective heat transfer problems', in *Finite Element Methods for Convection-Dominated Flows*, A.S.M.E. publication AMD, Vol. 34 (1979).
39. Segal, A., 'On the numerical solution of the Stokes equations using FEM', *Int. J. num. Meth. Engng*, **19**, 165 (1979).
40. Schneider, G., G. Raithby and M. Yavanovich, 'Finite element solution procedures for solving the incompressible, Navier–Stokes equations using equal order variable interpolation', *Num. Heat Transfer*, **1**, 433–451 (1978).
41. Bercovier, M. and O. Pironneau, 'Error estimates for the finite element solution of the Stokes problem in the primitive variables', *Numerische Math.*, **33**, 211 (1979).
42. Malkus, D. S., 'Eigenproblems associated with the discrete LBB condition for incompressible finite elements', *J. Eng. Sci.*, to appear.

DISCLAIMER